hepatocytes and collagen and was examined using light microscopy (DMR, Leica Co., Tokyo, Japan). For albumin immunostaining, the transverse section was permeabilized with 0.3% Triton X-100 in PBS for 10 min. Cells were incubated with 3 mL/L of H_2O_2 in methanol for 10 min to block endogenous peroxidase activity and then washed twice in PBS for 5 min. Nonspecific binding sites were blocked with 3 mL/L normal goat serum. Cells were incubated overnight at 4°C with primary antibody (goat anti-pig albumin antibody, Bethyl Lab, 1:200). After being washed for 15 min in PBS twice, slides were incubated at 37°C for 30 min with secondary antibody (anti-goat immunoglobulin G rhodamine-conjugated donkey antibody, Chemicon International, Temecula, CA), with streptavidin marked using horseradish peroxidase. The positive cells presented as brownish yellow.

Results

Isolation of hepatocytes

More than 2.5×10^9 hepatocytes were routinely obtained from a lobe. Viability determined according to the trypan blue exclusion method was higher than 90%.

Morphology of the monolayer-cultured hepatocytes

Three days after preservation in 0.25- or 0.025-mg/mL EGCG-containing medium, cells kept their morphologies and adhered to the culture dish, as shown in Figures 2B and C, whereas cells preserved in 0.0025 mg/mL and EGCG-free medium started to detach from the culture dish, as shown in Figures 2A and D. The number of detached cells in 0.0025-mg/mL EGCG-containing medium was much smaller than in EGCG-free medium. These results indicate that cellular damage in normal medium at room temperature leading to cell detachment can be prevented by adding EGCG to the medium.

Function of monolayer hepatocytes

The albumin production of the hepatocytes started to increase on the third day after isolation and reached the highest value on the fourth day, as shown in Figure 3. Albumin production rates slowly decreased over the culture period. During the preservation period, albumin production rates decreased drastically, to 0 μg/dish per day. After preservation in EGCG-containing medium, the cells were washed four times with culture medium to remove EGCG and incubated in a 5% CO_2/air atmosphere at 37°C for another 6 days. The highest albumin production was observed when the cells were preserved in the presence of 0.25-mg/mL EGCG.

Albumin production had increased to 14.5, 8.0, 1.1, and 8.9 μg/dish per day on the first day of post-preservation in 0.25-, 0.025-, and 0.0025-mg/mL EGCG-containing media and EGCG-free medium, respectively, as shown in Figure 3. Albumin production on the first day of post-preservation in EGCG-free medium was high, probably because of albumin released from the dead hepatocytes and not because of the albumin secretion process. The albumin production of hepatocytes preserved in 0.25-mg/mL EGCG-containing medium had drastically increased, up to a maximum rate of 30.9 μg/dish per day, on the third day of the post-preservation period, which was much higher than in the other conditions. The effect of EGCG concentration on the relative albumin production rate during the post-preservation period was compared with that before preservation (Table 1). Relative albumin production rate was calculated as follows:

$$\text{Relative of albumin production rate} = \frac{\text{Average value of albumin production rate during post-preservation}}{\text{Albumin production rate before preservation}} \times 100$$

From Table 1, albumin production of hepatocytes after preservation increased with increasing EGCG concentration. Production after preservation in 0.25-mg/mL EGCG-containing medium completely recovered and reached 111 ± 25.1%, but the albumin production rates of hepatocytes preserved in 0.025- and 0.0025-mg/mL EGCG-containing medium and EGCG-free medium recovered only to 74 ± 32.1, 58 ± 21.9, and 36 ± 23.7% of their pre-preservation levels, respectively.

The ammonium metabolism rate for hepatocytes preserved in EGCG-containing medium also recovered and reached higher levels than that of the hepatocytes preserved in EGCG-free medium (Fig. 4). Relative ammonium metabolism rate was calculated as follows:

$$\text{Relative of ammonium metabolism rate} = \frac{\text{Average value of ammonium metabolism rate during post-preservation}}{\text{Ammonium metabolism rate before preservation}} \times 100$$

The relative ammonium metabolism rates in hepatocytes preserved in 0.25-, 0.025-, and 0.0025-mg/mL EGCG-containing medium and EGCG-free medium after preservation were 52 ± 11.5%, 40 ± 8.3%, 53 ± 21.1%, and 17 ± 23.8%, respectively, compared to the rate before preservation, as shown in Table 2. These results indicate that maintaining the ammonium metabolism functions of hepatocytes in the monolayer culture is difficult even in the presence of EGCG.

Function of hepatocytes in 3D bioreactor

As shown in Figure 5A, albumin production of hepatocytes in the bioreactor reached a maximum rate (25.8 mg/reactor per day) at 4 days of pre-preservation culture. During the preservation period, albumin production decreased almost to 0 mg/reactor per day on the eighth day of culture. Albumin production increased during post-preservation culture and reached a maximum rate of 24.6 mg/reactor per day in 5 days, which is 72 ± 16% recovery relative to the rate observed before preservation. The ammonium metabolism rate after preservation was almost the same as that for pre-preservation, as shown in Figure 5B.

TABLE 1. RELATIVE ALBUMIN PRODUCTION OF MONOLAYER-CULTURED HEPATOCYTES

Culture	*EGCG Concentration (mg/mL)*	*Relative Albumin Production (%)*
Before-Preservation	—	100 ± 37.8
Post-Preservation	0	36 ± 23.7
	0.0025	58 ± 21.9
	0.025	74 ± 32.1
	0.25	111 ± 25.1

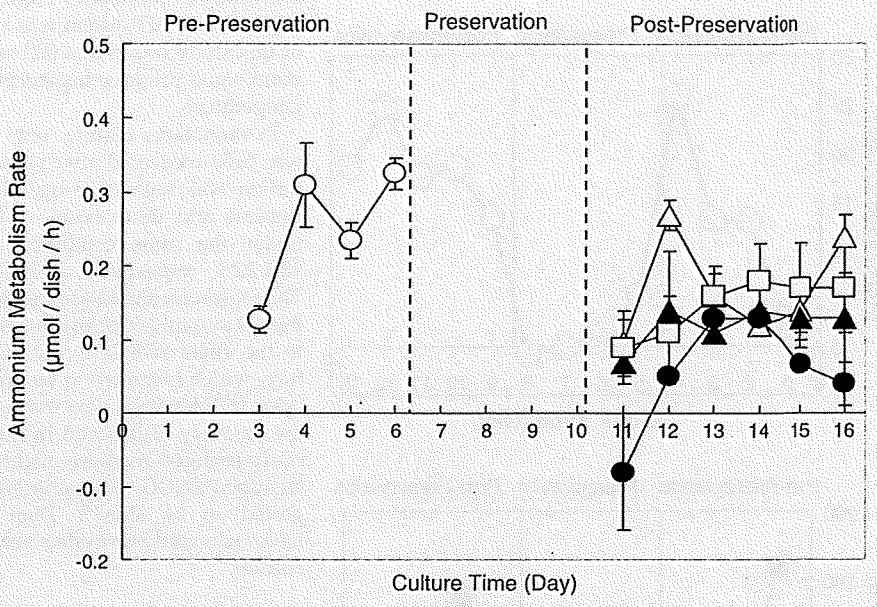

FIG. 4. Ammonium metabolism rate of monolayer-cultured hepatocytes during pre-preservation (○); preservation in epigallocatechin-3-gallate (EGCG)-free medium (●) and in 0.0025- (△), 0.025- (▲), and 0.25-mg/mL EGCG-containing medium (□).

The maximum rates of ammonium metabolism before preservation and after preservation were 167 μmol/reactor per hour and 149 μmol/reactor per hour, respectively, whereas the minimum rates before preservation and after preservation were 92 μmol/reactor per hour and 64 μmol/reactor per hour, respectively. The 3D bioreactor system is much more effective at maintaining the ammonium metabolic activity of the hepatocytes than the monolayer culture (Fig. 4), which is an almost 100% (98 ± 32%) recovery relative to the rate observed before preservation.

SEM and histological observation for perfusion culture

The hepatocytes preserved in 0.25-mg/mL EGCG-containing medium and post-cultured for 5 days produced extracellular matrix (ECM) proteins and were covered by them (Fig. 6A). The aggregates of hepatocytes which have spheroid-like structure were surrounded by the ECM structure rather than adhering onto PAU-coated PTFE, as shown in Figure 6B. This result was similar to our previous report in which the hepatocytes were cultured continuously for 1 week (supplementary data 2).[7] In addition, fibrin-like fibers were observed on the ECM layer (Fig. 6A).

The difference between the hepatocytes adhering onto substrates in 2D culture and forming the spheroid-like structure would be related to the higher functions of hepatocytes in a 3D system.[33–35] This was also proven using H&E staining, Azan staining, and albumin immunostaining, as shown in Figures 7A, B, and C. These images indicate that hepatocytes producing albumin were located in the ECM layer composed of collagen.

TABLE 2. RELATIVE AMMONIUM METABOLISM OF MONOLAYER-CULTURED HEPATOCYTES

Culture	*EGCG Concentration (mg/mL)*	*Relative Ammonium Metabolism (%)*
Before-Preservation	—	100 ± 6.4
Post-Preservation	0	17 ± 23.8
	0.0025	53 ± 21.1
	0.025	40 ± 8.3
	0.25	52 ± 11.5

Discussion

Cho *et al.* reported that the viability of hepatocytes decreased to 60% of control when preserved at low temperature in University of Wisconsin (UW) and Euro-Collins (EC) solutions for 48 h.[36] Not only the hepatocytes, but also the other valuable cells generally lost their viability in preservation. For example, peripheral blood stem cells and hemopoietic progenitor cells lost more than 50% of their viability after 3 days preserved at room temperature.[37] When hepatocytes were preserved at room temperature in monolayer culture for 4 days, more than half of the hepatocytes died and detached from the culture dish (Fig. 2A). In contrast, cell detachment was almost completely prevented, and the functions of the hepatocytes could be preserved in 0.25-mg/mL EGCG-containing medium for 4 days at room temperature. Albumin production in static culture increased after preservation at room temperature with increasing EGCG concentration.

A mechanism of cell or tissue preservation using EGCG has not been clarified, but it has been considered to be related to the intrinsic characteristics of polyphenol, that is, its amphipathic property.[19,20,38] The amphipathic property of EGCG is feasible to pass through the plasma membrane and the polyphenol adsorbs to the cellular receptors because of the high affinity that polyphenol and protein have for one another.[38] They proposed a hibernation-like phenomenon of the cells or tissues. As the polyphenol reversibly leaves the cell membrane with the progression of time, the cell cycle will be resuming.[20,38]

Our final aim is to develop a 3D BAL system for clinical use. Because a bioreactor system needs a large amount of hepatocytes, the effect of EGCG on hepatocyte function was

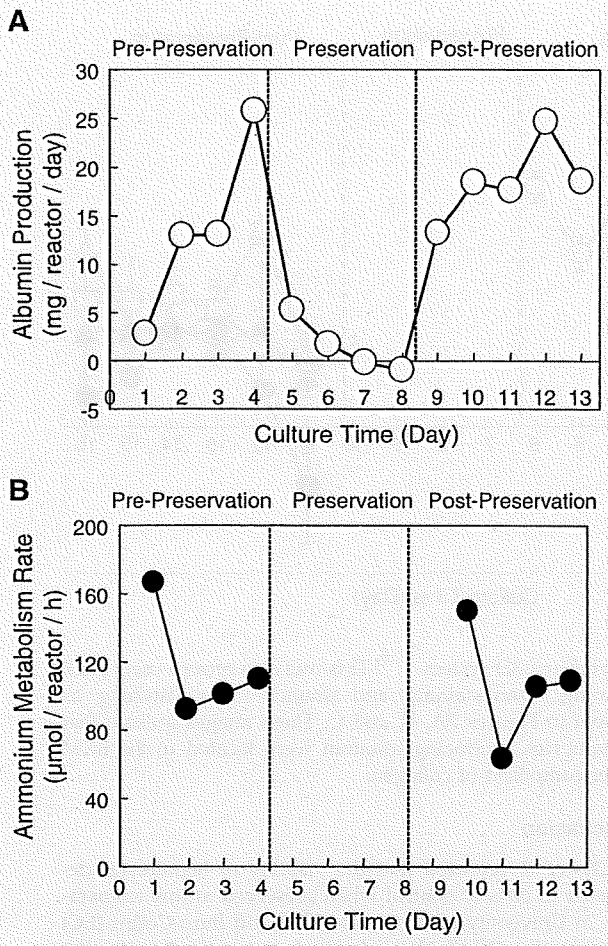

FIG. 5. Albumin production (A) and ammonium metabolism rate (B) of hepatocytes in three-dimensional bioreactor during pre-preservation, preservation in 0.25-mg/mL epigallocatechin-3-gallate–containing medium, and post-preservation.

confirmed in monolayer culture. Then, the concentration of EGCG in the 3D system was set to 0.25 mg/mL. The results of this study imply that 0.25-mg/mL EGCG-containing medium could preserve hepatocyte function for 4 days at room temperature.

In monolayer culture, only the albumin production rate was fully recovered after preservation when EGCG concentration was high (0.25 mg/mL). In contrast, albumin production and ammonium metabolism in a 3D bioreactor under the same conditions recovered to $72 \pm 16\%$ and $98 \pm 32\%$, respectively, of their levels before preservation. The reason for the better result in ammonium metabolism in the 3D system is unclear but is considered to relate not only to the effect of EGCG, but also to the spheroid-like structure, which is known to be preferable condition for hepatocytes.[33–35] Medium flow may also play an important role for the recovery of function in the 3D bioreactor. The continuously perfused medium might have effectively removed the adsorbed EGCG, whose desorption from the cells was suggested to be slow.[20] Then hepatocyte function might have recovered more effectively in a 3D system than in static culture.

Conclusion

In conclusion, EGCG-containing medium were found to be able to maintain the cultured hepatocyte morphology and functions. This system is useful for BAL preparation. Nevertheless, further studies are required to characterize the full effects of EGCG on hepatocytes as well as on how to preserve the cultured hepatocytes for longer than 4 days.

Acknowledgments

This work was partly supported by Grant-in-Aid for Scientific Research (B) in the Ministry of Education, Culture, Sports, Science, and Technology. We thank Ms. Sachiyo Fujinobu for her outstanding technical assistance. The author would like to thank Ministry of Higher Education Malaysia and Tun Hussein Onn University of Malaysia for funding his study under the Academic Training Scheme.

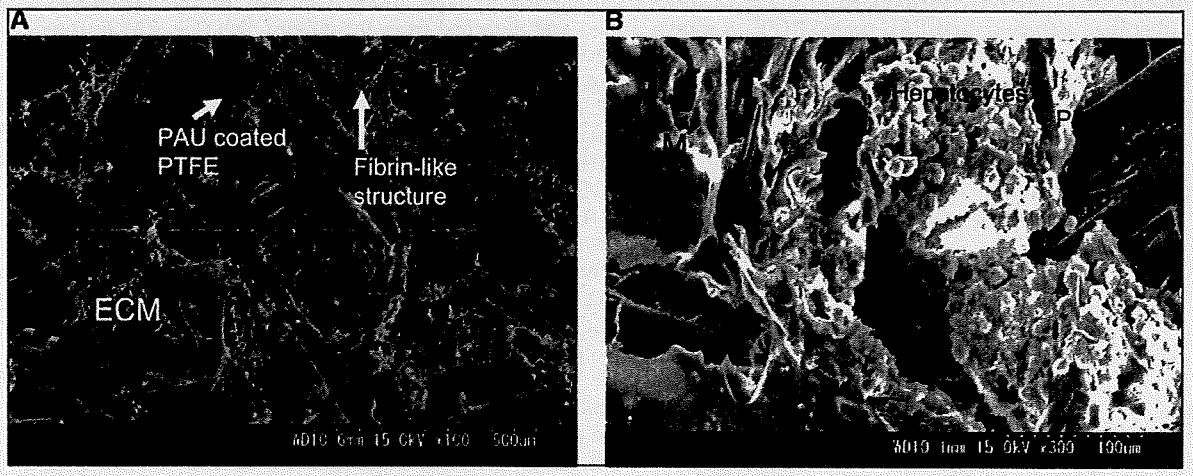

FIG. 6. Scanning electron microscopy photographs of hepatocytes preserved in the presence of 0.25-mg/mL epigallocatechin-3-gallate and cultured for 5 days in a bioartificial liver. (A) Extracellular matrix (ECM) and fibrin-like structures covering the non-woven fabric. (B) The aggregations of hepatocytes were observed under the ECM.

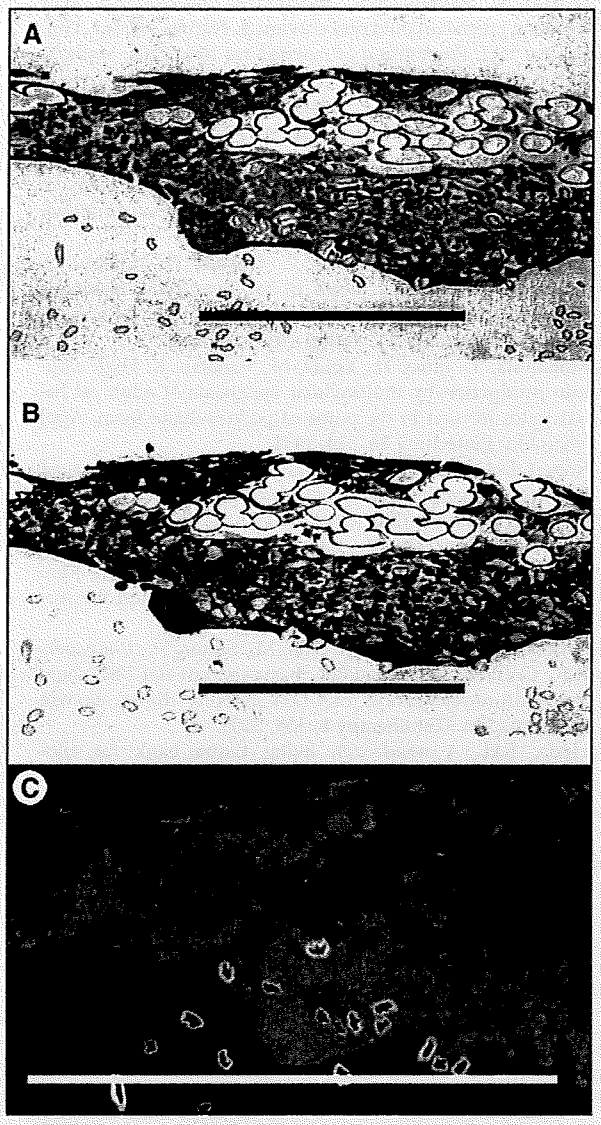

FIG. 7. (A) Hematoxylin and eosin staining, (B) Azan staining, and (C) albumin immunostaining of cultured hepatocytes in bioreactor. Cells were preserved in the presence of 0.25-mg/mL epigallocatechin-3-gallate for 4 days and cultured in normal medium for another 5 days. Bars represent 300 μm.

Disclosure Statement

No competing financial interests exist.

References

1. Demetriou, A.A., Brown, R.S., Busuttil, R.W., Fair, J., McGuire, B.M., Rosenthal, P., Am Esch, J.S. 2nd, Lerut, J., Nyberg, S.L., Salizzoni, M., Fagan, E.A., de Hemptinne, B., Broelsch, C.E., Muraca, M., Salmeron, J.M., Rabkin, J.M., Metselaar, H.J., Pratt, D., De La Mata, M., McChesney, L.P., Everson, G.T., Lavin, P.T., Stevens, A.C., Pitkin, Z., Solomon BA. Prospective, randomized, multicenter, controlled trial of a bioartificial liver in treating acute liver failure. Ann Surg **239,** 660, 2004.
2. Bilir, B.M., Guinette, D., Karrer, F., Kumpe, D.A., Krysl, J., Stephens, J., McGavran, L., Ostrowska, A., Durham, J. Hepatocyte transplantation in acute liver failure. Liver Transpl **6,** 32, 2000.
3. Baccarani, U., Sanna, A., Cariani, A., Barriga, M.S., Adani, G.L., Zambito, A.M., Piccolo, G., Risaliti, A., Nanni-Costa, A., Ridolfi, L., Scalamogna, M., Bresadola, F., Donini, A. Isolation of human hepatocytes from livers rejected for liver transplantation on a national basis: results of a 2-year experience. Liver Transpl **9,** 506, 2003.
4. Opolon, P. High permeability membrane hemodialysis and hemofiltration in acute hepatic coma. Experimental and clinical results. Artif Organs **3,** 354, 1979.
5. Millis, J.M., Cronin, D.C., Johnson, R., Conjeevaram, H., Conlin, C., Trevino, S., Maguire, P. Initial experience with the modified extracorporeal liver-assist device for patients with fulminate hepatic failure: system modifications and clinical impact. Transplantation **74,** 1735, 2002.
6. Terry, C., Dhawan, A., Mitry, R.R., Hughes, R.D. Cryopreservation of isolated human hepatocytes for transplantation: State of the art. Cryobiology **53,** 149, 2006.
7. Azizi, M., Noriko, S., Tetsuji, Y., Hiroshi, U., Makoto, K. Radial flow type bioreactor for bioartificial liver assist system using PTFE non-woven fabric coated with poly-amino acid urethane copolymer. Macromol Symp **249-250,** 151, 2007.
8. Innes, G.K., Fuller, B.J., Hobbs, K.E. Functional testing of hepatocytes following their recovery from cryopreservation. Cryobiology **25,** 23, 1988.
9. Pahernik, S.A., Thasler, W.E., Mueller-Hoecker, J., Schildberg, F.W., Koebe, H.G. Hypothermic storage of pig hepatocytes: Influence of different storage solution and cell density. Cryobiology **33,** 552, 1996.
10. Guillouzo, A., Rialland, L., Fautrel, A., Guyomard, C. Survival and function of isolated hepatocytes after cryopreservation. Chem Biol Interact **121,** 7, 1999.
11. Darr, T.B., Hubel, A. Postthaw viability of precultured hepatocytes. Cryobiology **42,** 11, 2001.
12. Yagi, T., Hardin, J.A., Valenzuela, Y.M., Miyoshi H., Gores, G.J., Nyberg, S.L. Caspase inhibition reduces apoptotic death of cryopreserved porcine hepatocytes. Hepatology **33,** 1432, 2001.
13. Rauen, U., Kerkweg, U., Weisheit, D., Petrat, F., Sustmann, R., Herbet, D.G. Cold-induced apoptosis of hepatocytes: Mitochondrial permeability transition triggered by non-mitochondrial chelatable iron. Free Radic Biol Med **35,** 12, 1664, 2003.
14. Muller, P., Aurich, H., Wenkel, R., Schaffner, I., Wolff, I., Walldorf, J., Fleig, W.E., Christ, B. Serum-free cryopreservation of porcine hepatocytes. Cell Tissue Res **317,** 45, 2004.
15. Li, L., Li, C.M., Zhang, B.Y., Hu, M.D., Li, X.Y., Ran, J.H., Huang, M. Apoptosis of rat liver in cold preservation with custom-designed KYL solution. Hepatobiliary Pancreat Dis Int **6,** 497, 2007.
16. Lloyd, T.D.R., Orr, S., Skett, P., Berry, D.P., Dennison A.R. Cryopreservation of hepatocytes: a review of current methods for banking. Cell Tissue Bank **4,** 3, 2003.
17. Watts, P., Grant, M.H. Cryopreservation of rat hepatocytes monolayer cultures. Hum Exp Toxicol **15,** 30, 1996.
18. McKay, G.C., Henderson, C., Goldie, E., Connel, G., Westmoreland, C, Grant, M.H. Cryopreservation of rat hepato-

cyte monolayers: cell viability and cytochrome P450 content in post-thaw cultures. Toxicol *In Vitro* **16,** 71, 2002.
19. Ikeguchi, R., Kakinoki, R., Matsumoto, T., Yamakawa, T., Nakayama, K., Morimoto, Y., Nakamura, T. Successful storage of peripheral nerves using University of Wisconsin solution with polyphenol. J Neurosci Methods **159,** 57, 2007.
20. Hyon, S.H., Kim, D.H. Long-term preservation of rat pancreatic islet under physiological conditions. J Biotechnol **85,** 241, 2001.
21. Tipoe, G.L., Leung, T.M., Hung, M.W., Fung, M.L. Green tea polyphenols as an anti-oxidant and anti-inflammatory agent for cardiovascular protection. Cardiovasc Hematol Disord Drug Targets **7,** 135, 2007.
22. Neuhaus, T., Voit, S., Lill, G., Vetter, H., Schor, K., Weber, A.A. Platelet aggregation induced by the C-terminal peptide of thrombospondin-1 (4N1-1) is inhibited by epigallocatechin gallate but not by prostaglandin E1. Platelets **15,** 455, 2004.
23. Ivanov, V., Roomi, M.W., Kalinovsky, T., Niedzwiecki, A., Rath, M. Anti-atherogenic effects of a mixture of ascorbic acid, lysine, proline, arginine, cysteine, and green tea phenolics in human aortic smooth muscle cells. J Cardiovasc Pharmacol **49,** 140, 2007.
24. Omasa, M., Fukuse, T., Matsuoka, K., Hyon, S.H., Wada, H. Effect of green tea extracted polyphenol on ischemia/reperfusion injury after cold preservation of rat lung. Transplant Proc **35,** 138, 2003.
25. Lee, S.R., Suh, S.L., Kim, S.P. Protective effects of the green tea polyphenol (-)-epigallocatechin gallate against hippocampal neuronal damage after transient global ischemia in gerbils. Neurosci Lett **287,** 191, 2000.
26. Varilek, G.W., Yang, F., Lee, E.Y., Villiers, W.J.S.D., Zhong, J., Oz, H.S., Westberry, K.F., McClain, C.J. Green tea polyphenol extract attenuates inflammation in interleukin-2-deficient mice, a model of autoimmunity. J Nutr **131,** 2034, 2001.
27. Ahmad, N., Gupta, S., Mukhtar, H. Green tea polyphenol epigallocatechin-3-gallet differentially modulates nuclear factor kB in cancer cells versus normal cells. Arch Biochem Biophys **376,** 2, 338, 2000.
28. Hayek, T., Fuhrman, B., Vaya, J., Rosenblat, M., Belinky, P., Coleman, R., Elis, A., Aviram, M. Reduced progression of atherosclerosis in apolipoprotein e-deficient mice following consumption of red wine, or its polyphenols quercetin or catechin, is associated with reduced susceptibility of LDL to oxidation and aggregation. Arterioscler Thromb Vasc Biol **17,** 2744, 1997.
29. Jankun, J., Selman, S.H., Swiercz, R., Jankun, E.S. Why drinking green tea could prevent cancer. Nature **387,** 561, 1997.
30. Seglen, P.O. Preparation of isolated rat liver cells. Methods Cell Biol **13,** 29, 1976.
31. Moldeus, P., Hogberg, J., Orrenius, S. Isolation and use of liver cells. Methods Enzymol **52,** 60, 1978.
32. Schwerer, B., Bach, M., Bernheimer, H. ELISA for determination of albumin in the nanogram range: assay in cerebrospinal fluid and comparison with radial immunodiffusion. Clin Chim Acta **163,** 237, 1987.
33. Landry, J., Bernier, D., Ouellet, C., Goyette, R., Marceau, N. Spheroidal aggregate culture of rat liver cells: histotypic reorganization, biomatrix deposition, and maintenance of functional activities. J Cell Biol **101,** 914, 1985.
34. Matsuhita, T., Ijima, H., Koide, N., Funatsu, K. High albumin production by multicellular spheroids of adult rat hepatocytes formed in the pores of polyurethane foam. Appl Microbiol Biotechnol **36,** 324, 1991.
35. Robert, R.A. Soames, A.R. Hepatocyte spheroids: prolonged hepatocyte viability for *in vitro* modeling of nongenotoxic carcinogenesis. Fundam Appl Toxicol **21,** 149, 1993.
36. Cho, H.R., Choi, D.H., Ko, B.K., Nam, C.W., Park, K.M., Lee, Y.J., Lee, S.G., Lee, J.S., Lee, K.A., Lee, E.A., Ju, S.A., Kim, B.S. Cold preservation of rat cultured hepatocytes: the scoparone effect. Transplant Proc **32,** 2325, 2000.
37. Antonenas, V., Garvin, F., Webb, M., Sartor, M., Bradstock, K.F., Gottlieb, D. Fresh PBSC harvests, but not BM, show temperature-related loss of CD34 viability during storage and transport. Cytotherapy **8,** 158, 2006.
38. Hyon, S.H. A non-frozen living tissue bank for allotransplantation using green tea polyphenols. Yonsei Med J. **45,** 1025, 2004.

Address reprint requests to:
Tetsuji Yamaoka, Ph.D.
Department of Biomedical Engineering
Advanced Medical Engineering Center
National Cardiovascular Center Research Institute
5-7-1 Fujishirodai, Suita
Osaka 565-8565
Japan

E-mail: yamtet@ri.ncvc.go.jp

Received: August 14, 2008
Accepted: November 20, 2008
Online Publication Date: January 13, 2009

J Artif Organs (2009) 12:111–117
DOI 10.1007/s10047-009-0449-4

ORIGINAL ARTICLE

Azizi Miskon, MEng · Tomo Ehashi, PhD
Atsushi Mahara, PhD · Hiroshi Uyama, PhD
Tetsuji Yamaoka, PhD

Beating behavior of primary neonatal cardiomyocytes and cardiac-differentiated P19.CL6 cells on different extracellular matrix components

Abstract Stem cell-based therapy in cardiac tissue engineering is an emerging field that shows great potential for treating heart diseases. However, even preliminary issues, such as the ideal niche for cardiomyocytes, have not been clarified yet. In the present study, the effects of extracellular matrix (ECM) components on the beating duration of neonatal rat cardiomyocytes (RCMs) and on the cardiac differentiation of P19.CL6 carcinoma stem cells were studied. RCMs were cultured on gelatin-, fibronectin-, and collagen type I-coated dishes and on noncoated polystyrene dishes, and their beating rate, beating duration, and cardiac gene expression were evaluated. The beating period and the expression of troponin T type-2 (TNNT2) and troponin C type-1 (TNNC1) of cardiomyocytes cultured on gelatin-coated dishes were longer and higher than for those on dishes with other coatings. For the cardiac differentiation of P19.CL6 cells, troponin T type-2 expression on gelatin- and fibronectin-coated dishes was five times that on collagen type I-coated dishes or polystyrene dishes 11days after induction. These results indicate that a gelatin-coated surface has a high ability not only to maintain the cardiac phenotype but also to enhance cardiac differentiation.

Key words Extracellular matrix · Cardiomyocyte · Beating · Differentiation

Received: September 5, 2008 / Accepted: January 14, 2009

A. Miskon · T. Ehashi · A. Mahara · T. Yamaoka (✉)
Department of Biomedical Engineering, Advanced Medical Engineering Center, National Cardiovascular Center Research Institute, 5-7-1 Fujishiro-dai, Suita, Osaka 565-8565, Japan
Tel. +81-6-6833-5012 ext. 2637; Fax +81-6-6835-5476
e-mail: yamtet@ri.ncvc.go.jp

A. Miskon · H. Uyama
Department of Chemical Engineering, Osaka University, Osaka, Japan

Introduction

Cardiac tissue engineering, such as cardiomyocyte transplantation for patients with ischemic heart disease or dilated cardiomyopathies, is of great potential therapeutic value to enhance the contractile function of the failing heart. Recently, fetal or neonatal rat cardiomyocytes were reported to form mature cardiac tissue in syngeneic hearts, acutely injured myocardium, and granulation tissue in the heart.[1] However, the best cell sources for clinical cardiomyocyte transplantation are still under debate. In general, three types of potential cell sources have been proposed.[2] One is the allogeneic source, including human embryonic stem cells or fetal allogeneic cardiomyocytes, but there still remain ethical issues. Another is the transgenic source. Genetically engineered animal cardiomyocytes have been studied in an attempt to reduce the rejection reaction in vivo, which is still a long-term problem in recipients.

The most promising cell source is the autogeneic one. Isolating cardiomyocytes from patients' hearts is unrealistic at present, and autologous skeletal muscle precursors, fibroblasts, or mesenchymal stem cells have been studied so far.[3] However, since beating cardiomyocytes are more promising,[4] we have been trying to differentiate bone marrow mesenchymal stem cells (BMSCs) into "beating" cardiomyocytes. There is no certain induction method for BMSC differentiation into beating cardiomyocytes. Many researchers have observed cardiac gene expression in MSCs treated with various inducers[5–7] or passage numbers,[8] but they do not beat spontaneously. Wakitani et al. and Makino et al. reported that murine BMSCs were differentiated to beating cardiomyocyte-like cells in vitro by exposing them to DNA-demethylating agent 5-azacytidine.[5,6] This is in contrast with a report stating that functional cardiac cells and gene expression were not obtained by treatment with 5-azacytidine.[9]

Producing autologous beating cardiomyocytes is thus an attractive goal for cell-based therapy. The crucial part is how to differentiate cells to cardiomyocytes in vitro and how to maintain the beating. Various microenvironments surrounding the cells (niches) play important roles not only

in cell proliferation but also in cell differentiation. The effect of extracellular matrix (ECM) proteins such as collagen type I, collagen type IV, gelatin, laminin, fibronectin, Matrigel (a mixture of laminin, collagen type IV, heparan sulfate proteoglycans, and entactin), and Cardiogel (a mixture of collagen types I and III, glycoproteins, laminin, fibronectin, and proteoglycans) on cell viability, proliferation rate, and cardiomyocyte gene expression have been reported;[10,11] however, the cardiomyocyte beating behavior has not fully been discussed.

In the present study, differentiation to beating cardiomyocytes and the beating duration of the cardiomyocytes were studied using two types of model cells. Murine embryonal carcinoma (EC) stem cells (P19.CL6),[12] which are widely used for investigating cardiac differentiation, were treated with differentiation medium containing 1% dimethyl sulfoxide (DMSO) on various ECM proteins (collagen, type I gelatin, and fibronectin), and their differentiation efficiency was evaluated. The effect of these substrates on the beating duration of rat neonatal cardiomyocytes was also investigated, along with intracellular cardiac marker genes [troponin T type-2 (TNNT2) and troponin C type-1 (TNNC1)][13] and skeletal muscle marker gene [troponin C type-2 (TNNC2)], which is reported to be expressed in the early developing heart.[14] Any fundamental information obtained would be important for the cardiac differentiation of various stem cells, including autologous BMSCs.

Materials and methods

Cardiomyocytes

Cardiomyocytes were isolated from neonatal Sprague–Dawley rat heart (1 to 2 days old) by the collagenase digestion method with modifications.[15,16] Institutional guidelines for the care and use of laboratory animals were observed. The hearts were removed and carefully minced with a scalpel blade into fragments and were rinsed several times with Hanks' balanced salt solution (Sigma-Aldrich, St. Louis, MO, USA) to remove blood and cellular debris. The minced hearts were gently stirred in 50 ml collagenase solution [0.15 M Sodium Chloride (NaCl), 5.63 mM Potassium Chloride (KCl), 0.02 M 4-(2-hydroxyethyl)-1-piperazineethanesulfonic acid (HEPES), 0.02 M Sodium Hydrogen Carbonate ($NaHCO_3$), 3.74 mM Calcium Chloride Dihydrate ($CaCl_2{\cdot}2H_2O$), and 6.5×10^4 U collagenase (Wako, Osaka, Japan, Lot no: 06032W)] at 37°C for 30 min. The resulting cell suspension was filtered through a nylon cell strainer (BD Falcon, BD Biosciences, Bedford, MA, USA) with a 40-μm pore size and centrifuged at 78 g for 3 min.

Isolated cardiomyocytes (1.0×10^5) were cultured in minimum essential medium alpha medium (α-MEM, Gibco, Invitrogen, Grand Island, NY, USA) supplemented with 10% (v/v) fetal bovine serum (FBS, MP Biomedicals, Eschwege, Germany, lot no: 7297H), and 100 IU/l penicillin–streptomycin (Wako, Osaka, Japan) on 60-mm gelatin-(IWAKI, Asahi Glass, Tokyo, Japan), fibronectin-(BD Falcon, BD BioCoat, BD Biosciences), or collagen type I-coated dishes and noncoated polystyrene dishes (IWAKI).

Differentiation of P19.CL6 cells

Differentiation of P19.CL6 cells was performed as described by Ohkubo with modifications.[12] Briefly, P19.CL6 cells were plated at a density of 3.7×10^5 cells on 60-mm gelatin-, fibronectin-, or collagen type I-coated dishes or noncoated polystyrene dishes with a α-MEM supplemented with 10% (v/v) FBS containing 1% DMSO (Wako). As a control experiment, P19.CL6 cells were cultured with α-MEM supplemented with 10% (v/v) FBS without 1% DMSO. The medium was changed every 2 days.

Measurement of action potential

Cultured plates on which beating colonies appeared were placed on the stage of an inverted phase-contrast optical microscope (ZEISS, Axiovert 135, Munich, Germany) and action potentials were measured immediately by a conventional microelectrode. The measurements were conducted after 1, 2, and 3 weeks of cultivation. Silicon-coated Ag wire (A-M System, Carlsborg, WA, USA, 250 μm bare, 330 μm coated) was used as the microelectrode. The microelectrode was set in a micromanipulator system (MON-202D, Nikon Narishige, Tokyo, Japan) and connected to a bioelectric amplifier (AB-621G, Nihon Kohde, Osaka, Japan). The sensitivity and time constant of the bioelectric amplifier were set at 0.1 mV/div and 0.003 s. For the measurements, the microelectrode was adjusted using the micromanipulator until it was attached to the membrane of beating cells. The voltage difference was amplified by the bioelectric amplifier and was displayed and recorded using Chart 5 software (AD Instrument, Bella Vista, Australia).

Total RNA isolation and reverse transcription

Total RNAs of cardiomyocytes and DMSO-treated P19.CL6 cells cultured on various dishes were extracted by QuickGene RNA cultured cell kit S (Fujifilm Life Science, Tokyo, Japan) 4 weeks after culture and 11 days after culture, respectively.

First-strand cDNAs were synthesized using a mixture of $oligo(dT)_{18}$ primer. Total cellular RNAs (200 ng) were incubated with 2.5 μM $oligo(dT)_{18}$ primer at 70°C for 10 min to denature the RNA secondary structure and then incubated at 4°C to let the primer anneal to the RNA. A given amount of 5X RT buffer (Toyobo, Osaka, Japan) and 2.5 mM Deoxynucleotide Trisphasphate (dNTP) mixture (Takara Bio, Shiga, Japan) (4 μl) were added and incubated at 37°C for 5 min. The reverse transcriptase (100 Units, Toyobo) was added into the mixture and the reverse transcriptase (RT) reaction was extended at 37°C for 1 h. Then, the reac-

Table 1. Polymerase chain reaction primers used in this study

Genes	Sense	Antisense
TNNT2	5′-GAAACAGGATCAACGACAACCA-3′	5′-CGCCCGGTGACTTTGG-3′
TNNC1	5′-GATCTCTTCCGCATGTTTGACA-3′	5′-TGGCCTGCAGCATCATCTT-3′
TNNC2	5′-AGATCGAATCCCTGATGAAGGA-3′	5′-CATCTTCAGAAACTCGTCGAAGTC-3′
GAPDH	5′-CTACCCCCAATGTATCCGTTGT-3′	5′-TAGCCCAGGATGCCCTTTAGT-3′

GAPDH, Glyceraldehyde 3 phosphate dehydrogenase

Table 2. Summary of voltage potentials for cardiomyocytes cultured in several types of extracellular matrix-coated dishes

Substrate	Action potential (mV) [Beating rate (Hz)]		
	Day 7	Day 14	Day 21
Gelatin	6.7 ± 0.49 [1.2 ± 0.05]	6.6 ± 1.26 [1.3 ± 0.01]	3.1 ± 0.21[2.8 ± 0.03]
Fibronectin	1.1 ± 0.97 [1.1 ± 0.30]	6.9 ± 1.15 [1.3 ± 0.42]	2.8 ± 0.11[2.0 ± 0.11]
Collagen type-I	2.6 ± 0.35 [0.8 ± 0.02]	1.7 ± 0.03 [2.3 ± 0.05]	ND
Polystyrene	2.0 ± 0.75 [0.3 ± 0.04]	ND	ND

ND, not done

tion mixture was heated at 94°C for 5 min to inactivate the enzyme and cooled at 4°C for 15 min. The RNase (DNase-free, 0.5 μg, Roche Diagnostics, Mannheim, Germany) was added to the mixture and incubated at 37°C to remove the template of RNA.

Real-time quantitative polymerase chain reaction

Real-time quantitative polymerase chain reaction (PCR) was conducted with SYBR Green. Primers for PCR analysis for troponin T type-2, troponin C type-1, and troponin C type-2 were designed using Primer Express software (Perkin-Elmer Applied Biosystems, Warrington, UK). The primer sequences are shown in Table 1. The reaction mixtures contained 23.74 μl distilled water, 25 μl SYBR Green Realtime PCR master mix (Toyobo), 100 nM of each primer, and 0.26 μl cDNA. The thermal profile for PCR was 50°C for 2 min, followed by 95°C for 10 min, followed by 40 cycles of 15 s at 95°C and 1 min at 60°C. Distilled water 0.26 μl was used as a negative control PCR reaction to ensure the absence of template contamination in PCR reagents. The average threshold cycle (Ct) values of triplicate measurements were used for all subsequent calculations on the basis of the delta Ct method.

Results

Beating behavior of isolated cardiomyocytes

One week after culture, the action potential of cardiomyocytes on gelatin-coated dishes was higher than that for other conditions (Fig. 1), and the beating duration was also longer than that for other conditions. The action potential and beating rates on each matrix are summarized in Table 2. After 7 days of culture, the action potential was around 6.7 ± 0.49 mV for cardiomyocytes cultured on gelatin-coated dishes, 1.1 ± 0.97 mV on fibronectin-coated dishes, 2.0 ± 0.35 mV on collagen type I-coated dishes, and 2.0 ± 0.75 mV on noncoated polystyrene dishes. These results indicate that the beating rate on fibronectin-coated dishes, collagen type I-coated dishes, and noncoated polystyrene dishes were 84%, 61%, and 70% lower than the beating rate on gelatin-coated dishes after 1 week of cultivation.

After 14 days of culture, the action potential became 6.6 ± 1.26 mV on gelatin-coated dishes, 6.9 ± 1.15 mV on fibronectin-coated dishes, and 1.7 ± 0.03 mV on collagen type I-coated dishes. No beating was observed on noncoated polystyrene dishes after 2 weeks of cultivation. After 21 days of culture, the action potential was 3.1 ± 0.21 mV on gelatin-coated and 2.8 ± 0.11 mV on fibronectin-coated dishes. No action potential was detected on collagen type I-coated dishes and polystyrene dishes.

The beating rate of cardiomyocytes was also affected by the ECM proteins. After 7 days of culture, the beating rate of cardiomyocytes was 1.2 ± 0.05 Hz on gelatin-coated dishes, 1.1 ± 0.3 Hz on fibronectin-coated dishes, 0.8 ± 0.02 Hz on collagen type I-coated dishes, and 0.3 ± 0.04 Hz on noncoated polystyrene dishes. After 14 days of culture, the beating rate became 1.3 ± 0.01 Hz on gelatin-coated dishes, 1.3 ± 0.42 Hz on fibronectin-coated dishes, and 2.3 ± 0.05 Hz on collagen type I-coated dishes. After 21 days, the beating rate was 2.8 ± 0.03 Hz on gelatin-coated dishes and 2.0 ± 0.11 Hz on fibronectin-coated dishes, whereas cardiomyocytes cultured on noncoated polystyrene dishes and collagen-coated dishes did not beat well and stopped at an early stage of cultivation. These results indicate that gelatin could maintain the beating behavior of cardiomyocytes for a longer time compared to fibronectin or collagen type I.

Expression of troponin T type-2 and troponin C type-1

Cardiac troponin T type-2 and troponin C type-1 are known to be cardiomyocyte markers and are important in the structure of muscle tissue; they also play a role in the contraction of muscle cells.[13] After 4 weeks of culture,

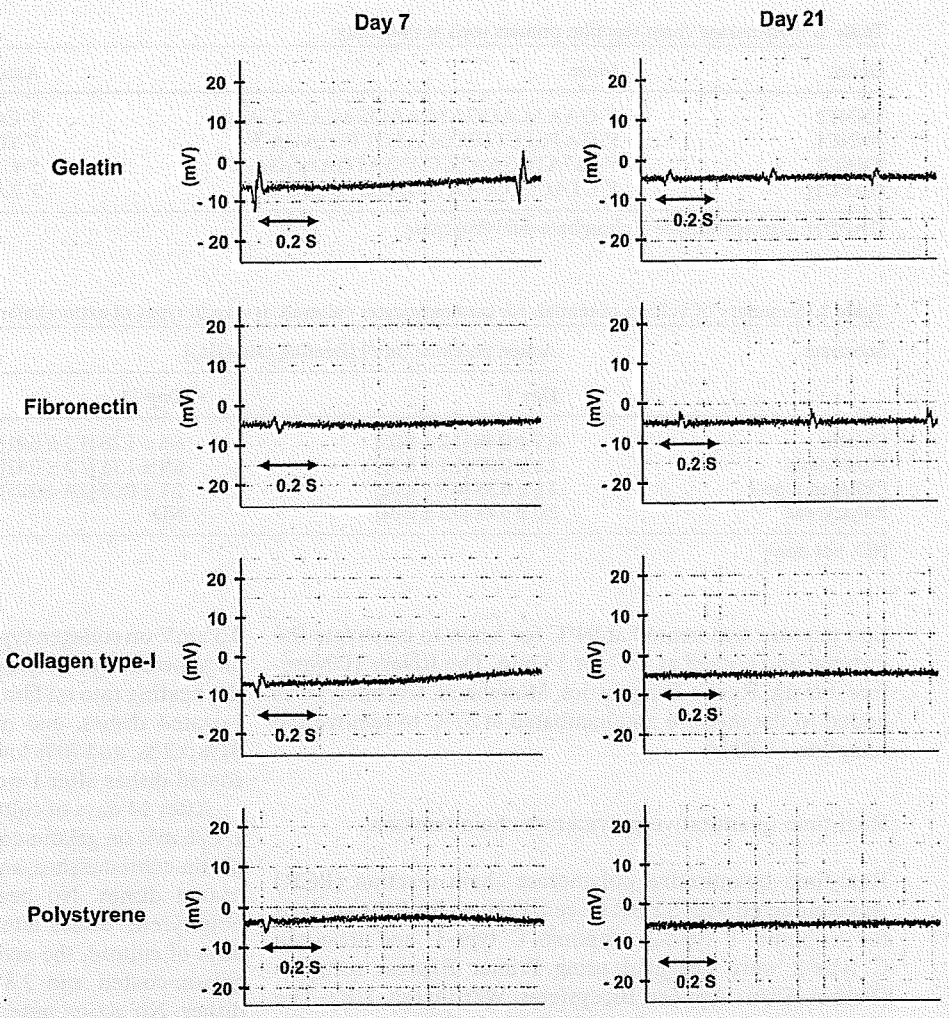

Fig. 1. Electrophysiological assessment of isolated cardiomyocytes after 7 and 21 days of cultivation on different substrates

expression of troponin T type-2 in cardiomyocytes on gelatin-coated dishes was 7, 6, and 12 times higher than those on fibronectin-coated, collagen-coated, and non-coated dishes (Fig. 2A). Expression of troponin C type-1 on gelatin-coated dishes was also 5, 6, and 32 times higher than those on fibronectin-coated, collagen type I-coated, and noncoated dishes (Fig. 2B). These results are consistent with the results of the electrophysiological study (Fig. 1), in which the beating of cardiomyocytes still could be detected on gelatin- and fibronectin-coated dishes after 3 weeks of cultivation.

Differentiation of P19.CL6 cells

Beating colonies were found on gelatin-coated dishes in 9 days with α-MEM medium containing 1% DMSO. This was followed by cells cultured on fibronectin-coated dishes after 10 days of culture and collagen type I-coated dishes after 11 days of culture. The average number of beating colonies found on the first day of detection was 13 ± 7 colonies per dish on gelatin-coated dishes, 9 ± 5 colonies per dish on fibronectin-coated dishes, 5 ± 2 colonies on collagen type I-coated dishes, and 3 ± 1 colonies on polystyrene dishes (Table 3).

As described earlier, troponin T type-2 and troponin C type-1 are known to be markers of cardiomyocytes,[13] and troponin C type-2 is reported to be a marker of cardiac development.[14] Expression of troponin T type 2 on gelatin- and fibronectin-coated dishes was higher than that for the other dishes, as shown in Fig. 3A. However, the expression of troponin C type-2 in collagen type I-coated dishes and noncoated polystyrene dishes was higher than that in gelatin- and fibronectin-coated dishes. The high expression of troponin C type-2 on collagen type I coated dishes and noncoated polystyrene dishes on day 11 was possibly because of the delayed differentiation of P19.CL6 cells to cardiomyocytes-like cells. Stoutamyer and Dhoot reported that troponin C type-2 was first expressed on day 3, reached maximum expression on day 5, and decreased day by day until no expression was found on day 11 during the development of quail heart in ovo.[14] Stoutamyer and Dhoot also reported that the expression of troponin C type-1 was detected on day 2 and decreased during the increase of

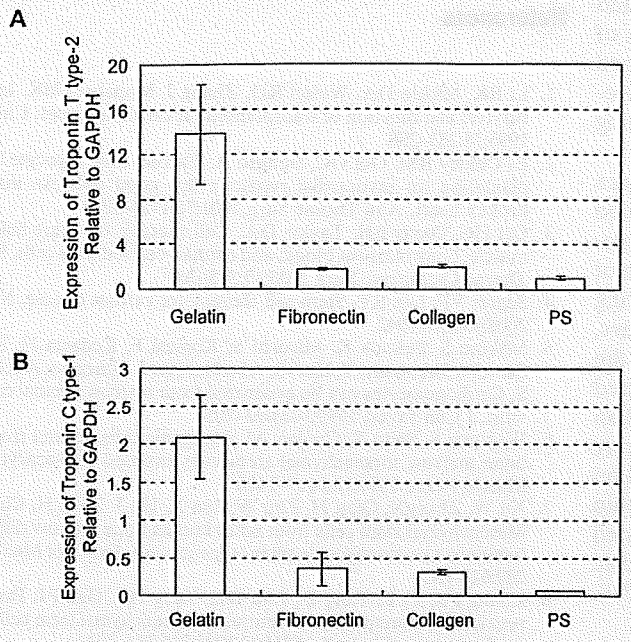

Fig. 2. Expression of cardiac markers (**A** troponin T type-2 and **B** troponin C type-1) in isolated cardiomyocytes after cultivation for 4 weeks on various types of extracellular matrix. *GAPDH*, Glyceraldehyde 3 phosphate dehydrogenase; *PS*, polystyrene

Table 3. Number of beating colonies of P19.CL6 cells 11 days after induction with 1% dimethyl sulfoxide

Substrate	Average number of beating colonies per dish
Gelatin	13 ± 7
Fibronectin	9 ± 5
Collagen type-I	5 ± 2
Polystyrene	3 ± 1

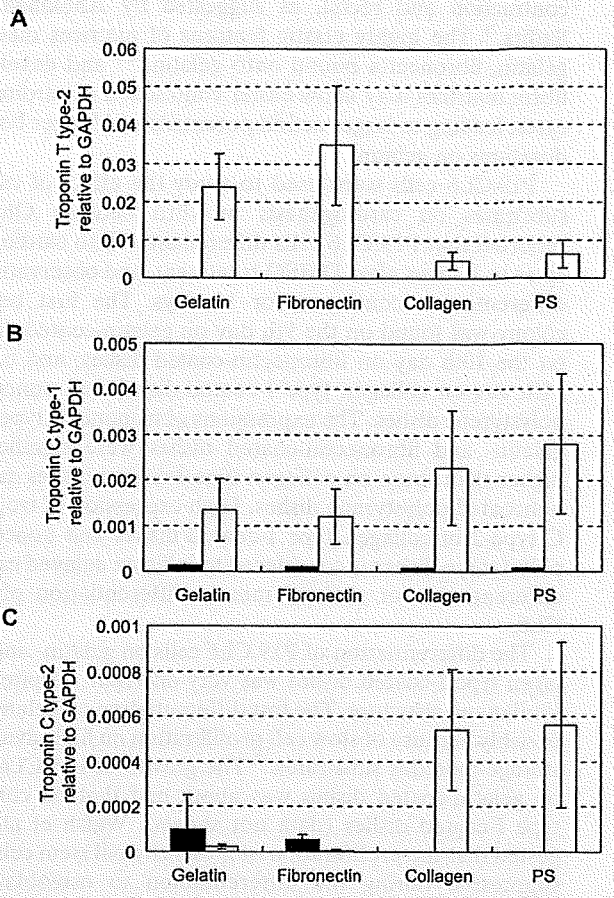

Fig. 3. Expression of cardiac markers in P19.CL6 cells (**A** troponin T type-2, **B** troponin C type-1, **C** troponin C type-2) treated with minimum essential medium alpha medium (α-MEM) containing 1% dimethyl sulfoxide on various dishes (*white bars*) or with α-MEM as a control for 11 days (*black bars*) PS, polysyrene

troponin C type-2, reaching a constant level after that.[14] In addition, the troponin C type-2 expression on a collagen-coated or noncoated dish may suggest skeletal muscle differentiation of P19.CL6 cells, although further analysis is needed.

These results demonstrated that differentiation of P19.CL6 cells to beating cells on gelatin-coated dishes and fibronectin-coated dishes was faster and more effective than that on collagen type I-coated dishes and noncoated polystyrene dishes.

Discussion

In the present study, enhanced action potentials and elongated beating durations of neonatal cardiomyocyte were observed on gelatin-coated dishes compared to those on collagen type I-coated dishes. Possible differences between gelatin and collagen are: (1) collagen posses a triple-helical conformation, (2) gelatin has a wide molecular weight distribution depending on its preparation process, (3) gelatin is easily hydrolyzed by protease,[17] (4) the dynamic storage modulus of gelatin is higher than that of collagen,[18] and (5) gelatin binds with fibronectin with a higher affinity.[19–21] It has already been reported that fibronectin is a very elastic substrate.[22]

The mechanism of the elongated beating duration on gelatin-coated substrate is unclear, but the mechanical properties (elasticity) and biological activity of the substrates might be influential. It has been reported that the mechanical properties of culture matrices affect various cellular properties such as the morphology of embryonic stem cells,[23,24] the collagen production of fibroblasts,[25,26] and the differentiation of mesenchymal and neural stem cells.[27,28]

Fibronectin produced by culture cells is known to associate with the fibronectin-binding domain of collagen, resulting in fibrillogenesis.[21] It has also been reported that fibronectin binds to gelatin more strongly than to collagen.[20,21] Therefore, the high production of fibrils might occur more effectively on gelatin-coated dishes than on fibronectin- or collagen-coated dishes. These connecting elastic fibers might regulate the motion of cardiomyocytes during

contraction and recoil, as suggested by Ahumada and Saffitz.[29] The highly elastic features of matrices made of gelatin, fibronectin bound onto gelatin,[18,22] and developed fibrin matrices may allow easier contraction of cardiomyocytes, leading to larger action potentials and longer beating durations on gelatin.

P19.CL6 cells were used to study the effect of culture substrates on cardiogenesis in vitro because Ohkubo reported that P19.CL6 cells differentiated into cardiomyocytes in 10 days after DMSO treatment, and observation of differentiation continued for 11 days. The first beating colony was found on the 9th day on gelatin-coated dishes, on the 10th day on fibronectin-coated dishes, and on the 11th day on collagen type I-coated dishes and noncoated polystyrene dishes. The expressions of troponin T type-2 on gelatin- and fibronectin-coated dishes were significantly higher than those on collagen type I-coated dishes and on noncoated polystyrene dishes. High expression of troponin C type-2 in collagen type I-coated dishes and noncoated polystyrene dishes is considered to indicate delayed cardiac differentiation or skeletal muscle differentiation of P19.CL6.

The differentiation of P19.CL6 cells on gelatin- and collagen type I-coated dishes was very different, despite their similar unit structure. The fast differentiation on gelatin was possibly because of slow cell proliferation on high-dynamic-storage-modulus substrates.[18] The growth of P19.CL6 cells on gelatin-coated dishes was about half that on collagen type I-coated dishes (data not shown). Walsh et al. suggested that the proliferation of mesenchymal stem cells was suppressed during the differentiation to osteoblasts in vitro.[30] The fast differentiation on fibronectin-coated dishes may also relate to the elasticity of the substrate.[22]

This finding will hopefully offer a bright future for the myocardial patch scaffold. It has been reported that the probability of cardiac differentiation of adipose tissue-derived mesenchymal stem cells after transplantation to infracted rat heart is quite low.[31] In the present study, the gelatin-based niche was found to be preferable for cardiac differentiation and for the beating function of cardiomyocytes. We will be applying these results to the cardiac differentiation of mesenchymal stem cells in order to prepare allogeneic beating cardiomyocytes.

Conclusion

The physical and biological properties of the substrate were the important factors not only for maintaining cardiac functions but also for leading to the cardiac differentiation of P19.CL cells. Gelatin was found to be a promising ECM protein to this end in vitro.

Acknowledgments This work was partly supported by a Grant-in-Aid for Scientific Research (B) from the Ministry of Education, Culture, Sports, Science and Technology of Japan. The author (Azizi Miskon) would like to thank the Ministry of Higher Education, Malaysia, and Tun Hussein Onn of the University of Malaysia for funding his study under the Academic Training Scheme.

References

1. Li RK, Mickle DA, Weisel RD, Zhang J, Mohabeer MK. In vivo survival and function of transplanted rat cardiomyocytes. Circ Res 1996;78:283–288
2. El Oakley RM, Ooi OC, Bongso A, Yacoub MH. Myocyte transplantation for myocardial repair: a few good cells can mend a broken heart. Ann Thorac Surg 2001;71:1724–1733
3. Ott HC, Davis BH, Taylor DA. Cell therapy for heart failure – muscle, bone marrow, blood, and cardiac-derived stem cells. Semin Thorac Cardiovasc Surg 2005;17:348–360
4. Segers VF, Lee RT. Stem-cell therapy for cardiac disease. Nature 2008;451:937–942
5. Makino S, Fukuda K, Miyoshi S, Konishi F, Kodama H, Pan J, Sano M, Takahashi T, Hori S, Abe H, Hata J, Umezawa A, Ogawa S. Cardiomyocytes can be generated from marrow stromal cells in vitro. J Clin Invest 1999;103:697–705
6. Wakitani S, Saito T, Caplan AI. Myogenic cells derived from rat bone marrow mesenchymal stem cells exposed to 5-azacytidine. Muscle Nerve 1995;18:1417–1426
7. Xu W, ZhangX, Qian H, Zhu W, Sun X, Hu J, Zhou H, Chen Y. Mesenchymal stem cells from adult human bone marrow differentiate into a cardiomyocyte phenotype in vitro. Exp Biol Med 2004; 229:623–631
8. Zhang FB, Li L, Fang B, Zhu DL, Yang HT, Gao PJ. Passage-restricted differentiation potential of mesenchymal stem cells into cardiomyocyte-like cells. BBRC 2005;336:784–792
9. Liu Y, Song J, Liu W, Wan Y, Chen X, Hu C. Growth and differentiation of rat bone marrow stromal cells: does 5-azacytidine trigger their cardiomyogenic differentiation? Cardiovasc Res 2003;58:460–468
10. Macfelda K, Kapeller B, Wilbacher I, Losert UM. Behavior of cardiomyocytes and skeletal muscle cells on different extracellular matrix components – relevance for cardiac tissue engineering. Artif Organs 2007;31:4–12
11. Bird SD, Doevendans PA, van Rooijen MA, Brutel de la Riviere A, Hassink RJ, Passier R, Mummery CL. The human adult cardiomyocyte phenotype. Cardiovasc Res 2003;58:423–434
12. Ohkubo AH. Differentiation of beating cardiac muscle cells from a derivative of P19 embryonal carcinoma cells. Cell Struct Funct 1996;21:101–110
13. Saggin L, Ausoni S, Gorza L, Sartore S, Schiaffino S. Troponin T switching in the developing rat heart. J Biol Chem 1998;263: 18488–18492
14. Stoutamyer A, Dhoot GK. Transient expression of fast troponin C transcripts in embryonic quail heart. J Muscle Res Cell Motil 2005;26:237–245
15. Seglen PO. Preparation of isolated rat liver cells. Methods Cell Biol 1976;13:29–83
16. Moldeus P, Högberg J, Orrenius S. Isolation and use of liver cells. Methods Enzymol 1978;52:60–71
17. Zhang Z, Li G, Shi B. Physicochemical properties of collagen, gelatin, and collagen hydrolysate derived from bovine limed split wastes. J Soc Leather Technol Chem 2006;90:23–28
18. Chien JC, Chang EP. Dynamic mechanical and rheo-optical studies of collagen and gelatin. Biopolymers 1972;11:2015–2031
19. Little CD, Chen WT. Masking of extracellular collagen and the co-distribution of collagen and fibronectin during matrix formation by cultured embryonic fibroblast. J Cell Sci 1982;55: 35–50
20. Engvall E, Ruoslahti E, Miller ED. Affinity of fibronectin to collagens of different genetic types and to fibrinogen. J Exp Med 1978;147:1584–1595
21. Dzamba BJ, Wu H, Jaenisch R, Peters DM. Fibronectin binding site in type I collagen regulates fibronectin fibril formation. J Cell Biol 1993;121:1165–1172
22. Erickson HP. Stretching fibronectin. J Muscle Res Cell Motil 2002;23:575–580
23. Bard JB, Hay ED. The behavior of fibroblasts from the developing avian cornea. Morphology and movement in situ and in vitro. J Cell Biol 1975;67:400–418
24. Hay ED. Interaction of embryonic surface and cytoskeleton with extracellular matrix. Am J Anat 1982;165:1–12

25. Nakagawa S, Pawelek P, Grinnell F. Extracellular matrix organization modulates fibroblast growth and growth factor responsiveness. Exp Cell Res 1989;182:572–582
26. Halliday NL, Tomasek JJ. Mechanical properties of the extracellular matrix influence fibronectin fibril assembly in vitro. Exp Cell Res 1995;217:109–117
27. Engler AJ, Sen S, Sweeney HL, Discher DE. Matrix elasticity directs stem cell lineage specification. Cell 2006;126:677–689
28. Saha K, Keung AJ, Irwin EF, Li Y, Little L, Schaffer DV, Healy KE. Substrate modulus directs neural stem cell behavior. Biophys J 2008;95:4426–4438
29. Ahumada GG, Saffitz JE. Fibronectin in rat heart: a link between cardiac myocytes and collagen. J Histochem Cyotchem 1984;4: 383–388
30. Walsh S, Jordan GR, Jefferiss C, Stewart K, Beresford JN. High concentrations of dexamethasone suppress the proliferation but not the differentiation or further maturation of human osteoblast precursors in vitro: relevance to glucocorticoid-induced osteoporosis. Rheumatology 2001;40:74–83
31. Miyahara Y, Nagaya N, Kataoka M, Yanagawa B, Tanaka K, Hao H, Ishino K, Ishida H, Shimizu T, Kangawa K, Sano S, Okano T, Kitamura S, Mori H. Monolayered mesenchymal stem cells repair scarred myocardium after myocardial infarction. Nat Med 2006;12: 459–465

In Vivo Tissue Response and Degradation Behavior of PLLA and Stereocomplexed PLA Nanofibers

Daisuke Ishii,[†,‡] Tang Hui Ying,[†,§,||] Atsushi Mahara,[⊥] Sunao Murakami,[⊥] Tetsuji Yamaoka,[⊥] Won-ki Lee,[▽] and Tadahisa Iwata*[,†,○]

Polymer Chemistry Laboratory, RIKEN Institute, 2-1 Hirosawa, Wako-shi, Saitama 351-0198, Japan, School of Biological Science, Universiti Sains Malaysia, 11800 Penang, Malaysia, Department of Biomedical Engineering, Advanced Medical Engineering Center, National Cardiovascular Center Research Institute, 5-7-1 Fujishirodai, Suita, Osaka 565-8565, Japan, and Division of Chemical Engineering, Pukyong National University, San 100, Yongdang-dong, Nam-gu, Busan 608-739, Republic of Korea

Received August 21, 2008; Revised Manuscript Received November 24, 2008

Biocompatibility of PLLA and stereocomplexed PLA nanofibers was evaluated by subcutaneous implantation in rats for 4−12 weeks. Characterization of the nanofibers was performed by GPC, SEM, wide-angle X-ray diffraction, and optical microscopy of hematoxylin-eosin stained ultrathin sections of explanted nanofibers. Stereocomplexed PLA nanofiber showed slower degradation than PLLA nanofiber and thus retained their shape after prolonged implantation. Furthermore, stereocomplexed PLA nanofiber caused milder inflammatory reaction than PLLA nanofiber. These results offer the potential use of PLLA and stereocomplexed PLA nanofibers as a biomaterial for short-term and long-term tissue regeneration, respectively. Stereocomplexed PLA nanofiber after in vitro degradation showed smaller degree of swelling than PLLA nanofiber. Taking the results of in vivo degradation together with in vitro degradation into consideration, bioabsorption mechanism of the in vivo degradation of the nanofibers is proposed.

Introduction

In the field of medical sciences, the method of tissue engineering has been extensively studied to overcome the problems of conventional methods such as organ transplantation and usage of artificial organs.[1] In tissue engineering, the proliferation and differentiation of cultured cells for deficiency repair has to be artificially controlled. The development of scaffold materials on which cells proliferate and differentiate has been a major concern in tissue engineering. Conventionally, collagens and gelatins extracted from animals have been used to produce scaffolds. However, the usage of these animal-origin materials is shrinking for fear of infectious diseases. Alternatively, the usage of biodegradable and biocompatible polymers that do not contain infectious substances such as endotoxins and prions has been explored.

Recently, as a novel method for producing scaffolds, formation of nanofibers with the diameter ranging from several tens to hundreds of nanometers is extensively studied.[2−4] Nanofiber scaffolds have fine pores and grooves as small as a few micrometers wide. Such fine structural features facilitate the adhesion and proliferation of cells. It is required for nanofiber scaffolds to sustain sufficient strength to support regenerating tissue cells and to be degraded after the tissue regeneration is completed. To meet these demands, various kinds of biodegradable and biocompatible polymers have been processed into nanofibers. Furthermore, the fiber morphology, crystalline structure, and degradation behavior of the nanofibers have been investigated.[5−7]

Poly(lactide) (PLA) is one of a few polymers that is practically applied as various medical materials such as implants and sutures.[8] PLA possesses mechanical properties sufficient to endure the mechanical load applied in human body. However, it is readily hydrolyzed both in enzymatic and nonenzymatic conditions.[9] The high susceptibility of PLA toward hydrolysis becomes a shortcoming when the long-time storage under physiological conditions is required. Various efforts to overcome this shortcoming have been attempted. One of such efforts is the formation of stereocomplex in PLA materials.

Stereocomplexed PLA is a characteristic crystalline form of PLA.[10,11] A sterically stable racemic crystal of stereocomplexed PLA is formed by complexing poly(L-lactide) (PLLA) and poly(D-lactide) (PDLA) that take molecular conformations of left-handed and right-handed helices, respectively.[12] As a result, stereocomplexed PLA has a melting temperature of 230 °C, that is 50 °C higher than PLLA and PDLA.[10] Furthermore, it has been reported that stereocomplexed PLA is more stable against hydrolysis than PLLA.[13−15] This finding offers the possibility for controlling the hydrolytic behavior of PLA material by the formation of stereocomplex. Although various methods have been proposed and investigated for the formation of stereocomplex within PLA materials,[16,17] PLA materials that contain only racemic crystal has not yet been processed. Furthermore, the conventional processes involve long-time annealing at elevated temperatures as high as 180 °C and repeated stretching. To form stereocomplexed PLA more conveniently, electrospinning has recently been applied to the formation of stereocomplexed

* To whom correspondence should be addressed. Tel.: +81-3-5841-7888. Fax: +81-3-5841-1304. E-mail: atiwata@mail.ecc.u-tokyo.ac.jp.
† RIKEN Institute.
‡ Present affiliation and address: Department of Materials Chemistry, Faculty of Science and Technology, Ryukoku University 1-5 Yokotani, Seta Oe-cho, Otsu-shi, Shiga 520-2194, Japan.
§ Universiti Sains Malaysia.
|| Present affiliation and address: Bioengineering Laboratory, RIKEN Institute, 2-1 Hirosawa, Wako-shi, Saitama 351-0198, Japan.
⊥ National Cardiovascular Center Research Institute.
▽ Pukyong National University.
○ Present affiliation and address: Graduate School of Agricultural and Life Sciences, The University of Tokyo, 1-1-1 Yayoi, Bunkyo-ku, Tokyo 113-8657, Japan.

10.1021/bm8009363 CCC: $40.75
Published on Web 12/31/2008

PLA.[18] In particular, we have first succeeded in processing sterecomplexed PLA nanofiber in which the racemic crystal is only the crystalline polymorph.[19] The formation of racemic crystal was performed by annealing the as-spun nanofiber at 100 °C, which is 80 °C lower than those in previously reported studies.

The degradation behavior of PLA nanofibers has been investigated by using various specimens and conditions.[20−22] However, the previous reports were all limited to in vitro conditions. There have been no reports on the biocompatibility and in vivo degradation behavior of stereocomplexed PLA nanofibers.

In this work, tissue responses and degradation behavior of PLLA and stereocomplexed PLA nanofibers in vivo were investigated by subcutaneously implanting these nanofibers in rats. The tissue response against the nanofibers has been investigated by means of histological observation. The changes in structure and properties of the nanofibers during subcutaneous implantation has been investigated using scanning electron microscopy (SEM), wide-angle X-ray diffraction (WAXD), gel permeation chromatography (GPC), and mechanical tensile testing. The relation between tissue response and degradation behavior of nanofibers is discussed in terms of the structural and property changes of the nanofibers.

Experimental Section

Materials. PLLA with a M_n of 4.7×10^5 and M_w/M_n of 1.8 was purchased from Polysciences, Inc. and used as received. PDLA with a $M_n = 2.2 \times 10^5$ and M_w/M_n of 1.5 was synthesized according to the following procedure. The D-lactide monomer, obtained from Purac, was recrystallized from anhydrous ethyl acetate. Bulk polymerizations were carried out in glass ampoules containing a magnetic stirring bar at 130 °C. Stannous octanoate in petroleum ether was used as the catalyst for the ring-opening polymerization. The ampoules were evacuated using a high vacuum pump and repeatedly flushed with high purity nitrogen to remove volatile impurities, solvents, and oxygen. Then the ampoules were sealed with a blowtorch and heated to the reaction temperature. The products in the ampoules were dissolved in chloroform, precipitated in the excess of methanol, filtered, and dried.

Electrospinning. Solutions of PLLA and PDLA (1 wt %) were prepared using 1,1,1,3,3,3-hexafluoro-2-propanol, HFIP, as the solvent. For the preparation of PLA stereocomplex nanofibers, equal volume of PLLA and PDLA solutions were mixed for several seconds by vortex mixer. Nanofibers were prepared using an Esprayer ES-2000 electrospinning device by Fuence, Co. Ltd. Dope solutions were extruded with a speed of 2.4 mL/h from a syringe needle with an inner diameter of 0.5 mm. Electrical voltage of 15 kV was applied to the syringe. Nanofibers were deposited onto a 10×10 cm^2 aluminum substrate placed perpendicular to the needle. To ensure sufficient thickness of nanofiber mats, the substrate was covered with a template made by a 51.4 μm thick Kapton film on which a 3×3 cm^2 window was opened. Distance between the needle tip and the substrate was set to 15 cm. The atmosphere of the spinning chamber was kept at less than 30% of relative humidity. PLLA and PLA stereocomplex nanofibers were then annealed in an oven at 100 °C for 8 h. Each electrospun PLA nanofiber mats was then cut into two different dimensions measuring 1×1 cm^2 and 1×3 cm^2, respectively. To prevent contamination, all scaffolds were sterilized overnight with ethylene oxide at 40 °C and kept in sealed bags until use.

Subcutaneous Implantation in Rat and Retrieval. Two 12-week old male Wistar rats were used for implanting the scaffolds; one for scaffolds measuring 1×1 cm^2, while the other for scaffolds measuring 1×3 cm^2. The experimental protocol had been approved by the Animal Care Committee of the National Cardiovascular Center, Osaka, Japan. The implantation of nanofiber mat was performed under anesthesia using diethyl ether. The 1×1 cm^2 scaffolds were implanted subcutaneously at one side of the backbone while the 1×3 cm^2 scaffolds were implanted subcutaneously at the backbone. The grouping of the rats was based on the duration of observation for 4 weeks and 12 weeks.

Upon explantation, the nanofiber mats measuring 1×1 cm^2 were excised with the surrounding tissues and stored in 2.5% glutaraldehyde in phosphate buffer saline (PBS) with a pH of 7 until further preparation of ultrathin section for histological observation. The retrieved 1×3 cm^2 nanofiber mats were treated with 1.25 wt % trypsin solution to remove the surrounding tissues. They were then kept in tubes containing PBS at 4 °C until further use. Trace amount of sodium azide was added to avoid the decay of the specimens. After trypsin treatment, surrounding tissues were manually removed as much as possible. The nanofiber mats were repeatedly washed using milli-Q water and dehydrated using ethanol series. Finally, the dehydrated nanofiber mats were dried overnight using vacuum desiccator at room temperature.

In Vitro Degradation. Nanofiber mats with the size of 1×3 cm^2 were incubated in 5 mL of PBS with a pH of 7.27 for 4−12 weeks at 37 °C. The medium was changed every 2 weeks. After 4 and 12 weeks of incubation, the nanofiber mats were washed thoroughly with distilled water, vacuum-dried at room temperature, and then subjected to SEM observation.

Histological Observation. The surrounding tissues were excised together with the implanted nanofiber mats and fixed with 2.5% glutaraldehyde in PBS with a pH of 7. A small piece of the tissue was then embedded in paraffin before subjecting it to microtome sectioning. Hematoxylin and eosin (HE) were used for staining the tissues. The tissue response to nanofiber mats was evaluated from the coloration observed with a phase-contrast microscope.

Scanning Electron Microscopy (SEM). Nanofiber mat was placed on a stub and then coated with Au. The thickness of Au coat was about 15 nm. SEM images of nanofibers were obtained using a field emission scanning electron microspope (JSM-6330F, JEOL, Co. Ltd.) operating at an acceleration voltage of 5 kV of and an emission current of 12 μA. For estimating the average diameter of nanofibers, diameter was measured at more than 60 points on the printed SEM image.

Wide-Angle X-ray Diffraction (WAXD). WAXD patterns of nanofiber mats were acquired under ambient condition using Rigaku RINT-2500 system operating at 40 kV and 200 mA. Measurements were performed on a Bragg−Brentano type $2\theta/\theta$ goniometer in a reflection mode. Ni-filtered Cu Kα radiation ($\lambda = 0.15418$ nm) was collimated with a 1/2 deg divergence slit, 1/6 deg scatter slit and 0.15 mm receiving slit. Scans were performed three times in a 2θ range of 10−40° with a scan rate of 0.5°/min and 0.05° step.

Gel Permeation Chromatography (GPC) Analysis. The molecular weight analysis of the nanofiber mats was performed with gel-permeation chromatography at 40 °C, using a Shimadzu LC-10A GPC system equipped with a RID-10A refractive index detector and Shodex K-806 M and K-802 columns. Chloroform was used as the eluent at a flow rate of 0.8 mL min^{-1}. The calibration curve was prepared by using monodisperse polystyrene standards.

Results

Changes in the Appearance of Nanofiber Mats During Subcutaneous Implantation. Figure 1a,b shows SEM images of the PLLA and stereocomplexed PLA nanofibers, respectively. Both nanofibers possess similar morphology with the average fiber diameter of about 300 nm. However, totally different crystalline structure is formed in these nanofibers, as seen from the WAXD profiles in Figure 1c. PLLA nanofiber shows diffraction peaks at $2\theta = 15.1$, 16.5 (assigned to (110)/(200)), and 18.1° that are assigned to α-form homocrystal of PLA.[12] On the other hand, stereocomplexed PLA nanofiber showed diffraction peaks at $2\theta = 12.0$ (assigned to (110)), 20.8, and 24.1° that are assigned only to stereocomplex crystal of PLA.[12]

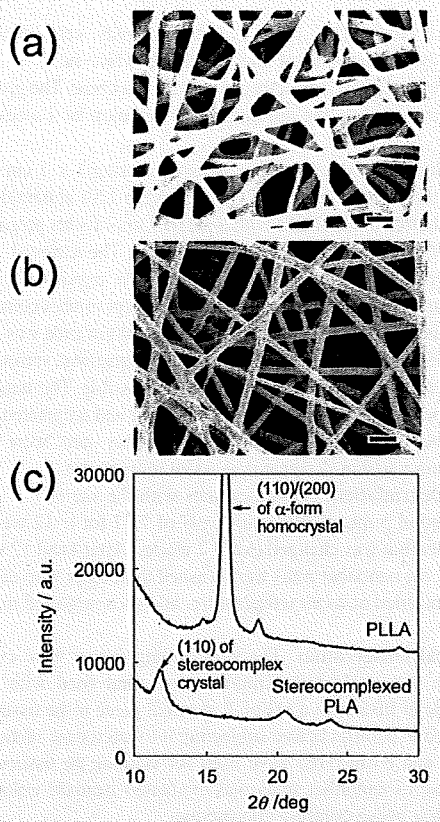

Figure 1. SEM images of (a) PLLA and (b) stereocomplexed PLA nanifibers and (c) wide-angle X-day diffraction patterns of PLLA and stereocomplexed PLA nanofibers. Scale bars = 1 μm. PLLA nanofiber shows diffraction peaks at 2θ = 15.1, 16.5 (assigned to (110)/(200)), and 18.1° that are assigned to α-form homocrystal of PLA. On the other hand, stereocomplexed PLA nanofiber showed diffraction peaks at 2θ = 12.0 (assigned to (110)), 20.8, and 24.1° that are aasigned only to stereocomplex crystal of PLA.

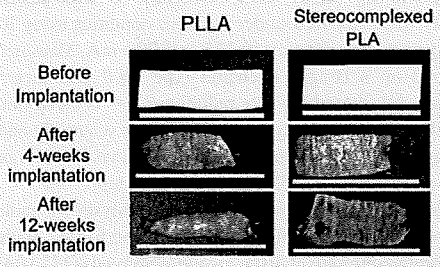

Figure 2. Bulk appearances of the nanofiber mats of PLLA and stereocomplexed PLA (a) before implantation, (b) after 4 weeks of implantation and (c) after 12 weeks of implantation. Scale bars = 3 cm.

This shows that the stereocomplexed PLA nanofiber consists of only the stereocomplex crystal and does not contain homocrystal of PLLA and PDLA at all.

The bulk appearances of the nanofiber mats were observed before and after removing the surrounding tissues. Figure 2 shows the photographs of nanofiber mats before and after 4 week and 12 week implantations, respectively. Significant reduction in the size of the PLLA nanofiber mat was recognized with the increasing period of implantation. In particular, the PLLA nanofiber mat after a 12 week implantation was densely covered with the surrounding tissues and only small fragments of the nanofibers mat were recovered. On the other hand, the stereocomplexed PLA nanofiber mat showed a less degree of the reduction in size than the PLLA nanofiber mat. This suggests

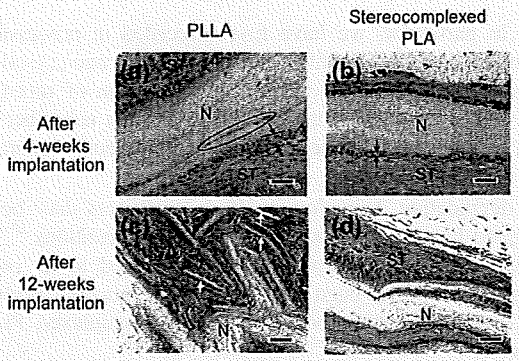

Figure 3. Histological images of PLLA and stereocomplexed PLA nanofibers before and after 4 weeks of implantation. (a) PLLA, before implantation; (b) stereocomplexed PLA, before implantation; (c) PLLA, after implantation; (d) stereocomplexed PLA, after implantation. Tissues were stained with hematoxylineosin. Nuclei of the inflammatory cells are stained blue. The width of inflammatory cells is indicated by the arrows and lines in (a) and (b). Ellipsoid region in (a) and white arrows in (c) indicate the infiltration of surrounding tissues and fragmented nanofibers, respectively. ST: surrounding tissues; N: nanofiber mats. Scale bars = 50 μm.

that the in vivo degradation of the stereocomplexed PLA nanofiber mat occurs slower than the PLLA nanofiber mat.

Histological Observation of Nanofiber Mats with the Surrounding Tissues. Histological observations of the nanofiber mats were performed to investigate the degree of inflammatory reactions and penetration of the surrounding tissues into the nanofiber mats. Figure 3 shows the phase contrast images of ultrathin sections of the explanted nanofiber mats stained by hematoxylin-eosin. The nuclei of inflammatory cells were stained blue by the hematoxylin dye and their presence is an indication of tissue response toward the implanted nanofiber mats. As indicated by the arrows and lines in Figure 3a, a thick layer of inflammatory cells was accumulated at the interface between the PLLA nanofiber mat and the surrounding tissues. In contrast, the layer of accumulated inflammatory cells was thinner for the stereocomplexed PLA nanofiber mat, as shown in Figure 3b. This indicates that the stereocomplexed PLA nanofiber mat causes smaller degree of inflammatory reactions than the PLLA nanofiber mat.

Furthermore, delamination (indicated by the ellipsoid in Figure 3a) occurred on the surface of the PLLA nanofiber mat, and hence, the infiltration of the surrounding tissues was observed. However, no infiltration of the surrounding tissues was observed for the stereocomplexed PLA nanofiber mat. After 12 weeks of implantation, while the PLLA nanofiber mat was significantly fragmented (white arrows indicate the fragmented nanofiber mat), the stereocomplexed PLA nanofibers retained the mat-like bulk morphology. These trends are well correlated with the bulk appearances of the nanofiber mats and support the observation that the in vivo degradation of the stereocomplexed PLA nanofiber mat proceeds slower than the PLLA nanofiber mat.

SEM Observation. SEM observation was performed for the nanofiber mats before and after 4 weeks and 12 weeks of implantation. Figure 4 shows the SEM images of nanofiber mats before implantation, after implantation and incubation at different periods of time. As for PLLA, cleavage of each strand of nanofiber occurred after 4 weeks. Furthermore, after 12 weeks, a decrease in the density of the nanofiber mat was observed. This is consistent with the histological image showing the fragmentation of the PLLA nanofiber mat. On the other hand, no cleavage of the stereocomplexed PLA nanofibers was observed even after 12 weeks of implantation.

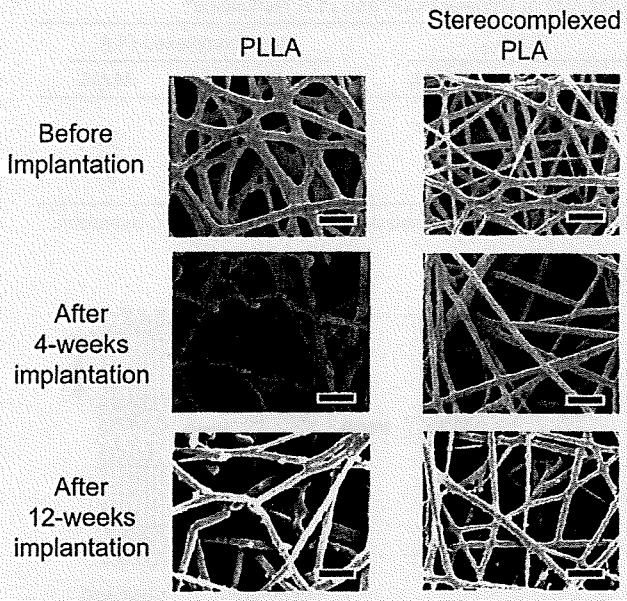

Figure 4. SEM images of PLLA (left) and stereocomplexed PLA (right) nanofibers. Upper row, before implantation; middle row, after 4 weeks of implantation; lower row, after 12 weeks of implantation. The surrounding tissues were removed by trypsin treatment. Scale bars = 1 μm.

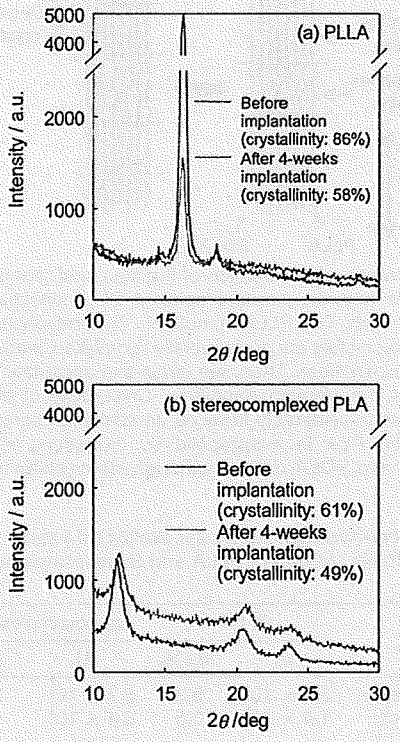

Figure 5. Wide-angle X-ray diffraction patterns of PLLA and stereocomplexed nanofibers before and after 4 weeks of implantation. PLLA nanofiber showed diffraction peaks at $2\theta = 15.1°$, 16.5°, and 18.1° that are assigned to homopolymer crystal of PLLA. On the other hand, stereocomplexed PLA nanofiber showed diffraction peaks at $2\theta = 12.0$, 20.8, and 24.1° that are assigned to stereocomplexed crystal. No diffraction peaks assigned to homopolymer crystal were observed in stereocomplexed PLA nanofiber.

Changes in Crystallinity. Figure 5 shows the WAXD patterns of the PLLA and stereocomplexed PLA nanofibers before and after 4 weeks of implantation. While the PLLA nanofiber showed diffractions that are assigned to the α-form

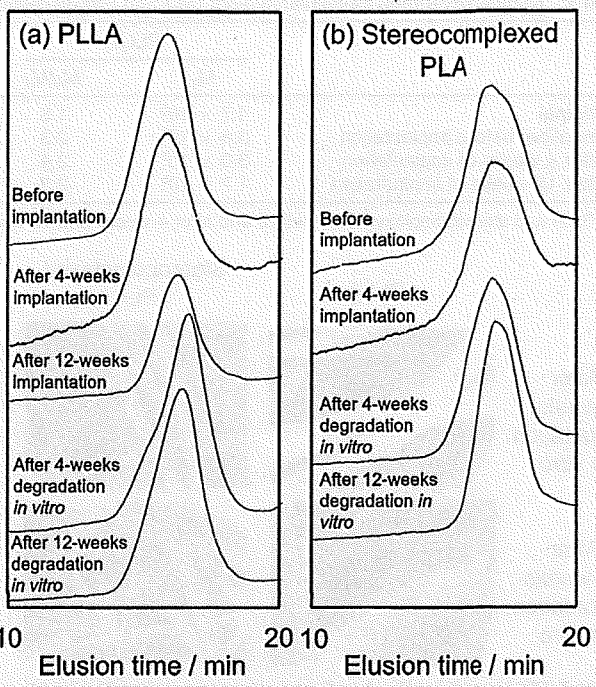

Figure 6. GPC elusion profiles of (a) PLLA and (b) stereocomplexed PLA nanofibers before and after implantation in vivo for 4 weeks and 12 weeks and before and after in vitro degradation for 4 weeks and 12 weeks.

crystal of PLA, the stereocomplexed PLA nanofiber showed diffractions assigned only to stereocomplexed crystal.[12] The crystallinity of both nanofibers was calculated as the ratio between the integrals of crystalline diffraction intensity and the total diffraction intensity. While the PLLA nanofiber showed considerable decrease in its crystallinity from 86 to 58%, the stereocomplexed PLA nanofiber showed a smaller decrease from 61 to 49%. These results show that the crystallinity of the stereocomplexed PLA is not so much lowered by implantation, while that of PLLA nanofiber significantly decreases. These results support the higher stability of stereocomplexed PLA nanofiber than PLLA nanofiber, as seen from visual inspection of the explanted nanofiber mat and the histological observation.

GPC Analysis. The possibility of the cleavage of molecular chains during implantation, as suggested from SEM and WAXD data, was investigated by GPC analysis. The GPC elusion profiles are shown in Figure 6. Table 1 shows the number-averaged molecular weight, M_n, and the polydispersity index, M_w/M_n, of the PLLA and stereocomplexed PLA nanofibers before and after 4 weeks of implantation. Data for original PLLA are also shown in Table 1. In the case of 12 weeks, GPC data of stereocomplexed PLA were not obtained because of its low solubility in chloroform. PLLA nanofiber showed a decrease in M_n during the implantation. In contrast, the M_n of stereocomplexed PLA nanofiber remained unchanged despite the decrease in M_w/M_n for 4 weeks of implantation. These results indicate that stereocomplexed PLA was not degradaded during implantation, while the PLLA chains in the nanofiber were considerably degraded. Additionally, in the case of the stereocomplexed PLA nanofiber, the extraction of low molecular weight fraction might occur during implantation.

In Vitro Degradation. To consider the results obtained from the in vivo experiment in terms of biocompatibility and bioabsorption, changes in the structure and properties of the nanofibers after in vitro incubation were investigated. As seen in Figure 7, both PLLA and stereocomplexed PLA nanofibers

Table 1. Number-Averaged Molecular Weight (M_n) and Polydispersity Index (M_w/M_n) of Original PLLA and PLA Nanofibers[a]

	PLLA		PDLA		stereocomplexed PLA	
	M_n	M_w/M_n	M_n	M_w/M_n	M_n	M_w/M_n
original	4.7×10^5	1.8	2.2×10^5	1.5		
nanofiber before implantation	3.8×10^5	2.3			8.7×10^4	3.3
after 4 weeks of implantation	3.0×10^5	2.4			8.6×10^4	2.3
after 12 weeks of implantation	1.7×10^5	2.3			[b]	[b]

[a] PLLA and stereocomplexed PLA before and after 4 weeks and 12 weeks of implantation. [b] Not obtained due to the poor solubility in chloroform.

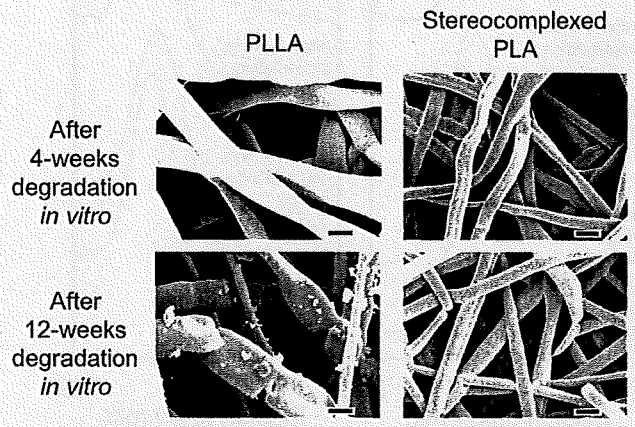

Figure 7. SEM images of PLLA (left) and stereocomplexed PLA (right) nanofibers after 4 weeks (upper) and 12 weeks (lower) in vitro degradation in PBS. Scale bars = 1 μm.

after in vitro incubation showed a considerable increase in the fiber diameter. This suggests that the significant swelling of the nanofibers occurred during the incubation. Interestingly, the stereocomplexed PLA nanofiber showed a smaller degree of swelling (from 300 to 600 nm) than the PLLA nanofiber (from 300 to 1200 nm). Because strong interaction works between molecular chains of PLLA and PDLA in the sterecomplexed PLA nanofiber, the swelling of the stereocomplexed PLA nanofiber might be suppressed.

GPC data of the nanofibers before and after in vitro degradation were also obtained, as shown in Figure 6b. The M_n and M_w/M_n estimated from the GPC curves are listed in Table 2. The M_n of stereocomplexed PLA was almost unchanged while that of PLLA showed a decrease from 3.8×10^5 to 1.8×10^5. These trends are consistent with the molecular weight data before and after the implantation in vivo as shown in Table 1.

The difference in the swelling behavior and molecular weight change in vitro between the stereocomplexed PLA and PLLA nanofibers may explain the results of the subcutaneous implantation in vivo in which the stereocomplexed PLA nanofiber showed smaller degree of absorption than the PLLA nanofiber.

Discussion

Degradation Mechanism of PLLA and Stereocomplexed PLA Nanofibers In Vivo. A schematic representation of the degradation mechanism of the PLLA and stereocomplexed PLA nanofibers is shown in Figure 8. For the PLLA nanofiber, it is believed that the molecular chains in the amorphous region between lamella crystals are preferentially hydrolyzed due to the intracrystalline swelling. This leads to the cleavage of a nanofiber and a decrease in the molecular weight. Then the chain-end degradation at the edge of the cleaved nanofiber may occur and lead to the decrease in the crystallinity. The cleavage of nanofiber may facilitate the delamination and the subsequent fragmentation of the nanofiber mats and, consequently, the

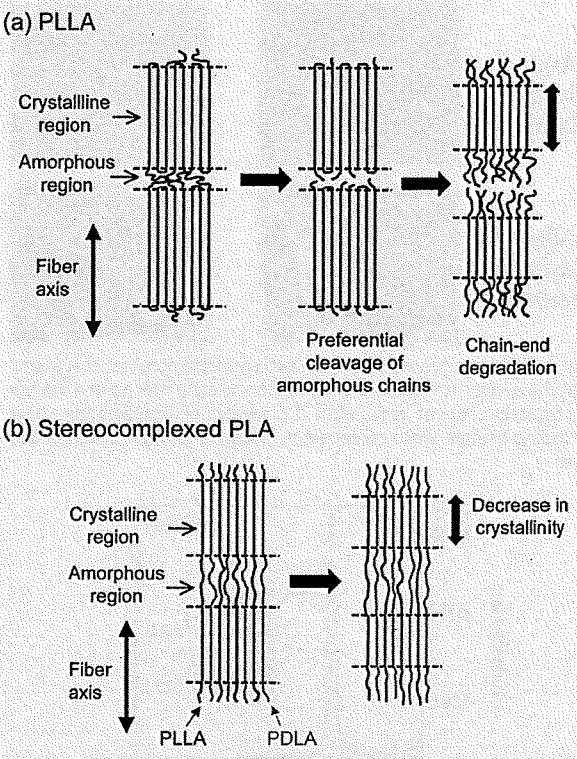

Figure 8. Schematic representation of the structural changes of (a) PLLA nanofiber and (b) stereocomplexed PLA nanofiber during implantation in vivo. For PLLA nanofiber, the amorphous chains between lamella crystals are preferentially hydrolyzed, leading to the cleavage of the nanofiber. Then, the chain-end degradation occurs at the edge of the cleaved nanofiber. Crystallinity of the PLLA nanofiber is thus considerably lowered. In contrast, degradation of stereocomplexed PLA is suppressed by the strong interaction between PLLA and PDLA chains, although the crystallinity slightly decreases.

Table 2. Number-Averaged Molecular Weight (M_n) and Polydispersity Index (M_w/M_n) of PLLA and Stereocomplexed PLA Nanofibers[a]

	PLLA		stereocomplexed PLA	
	M_n	M_w/M_n	M_n	M_w/M_n
before degradation	3.8×10^5	2.3	8.7×10^4	3.3
after 4 weeks of degradation	1.4×10^5	3.5	8.4×10^4	3.0
after 12 weeks of degradation	1.8×10^5	3.0	6.9×10^4	2.2

[a] Before and after 4 weeks and 12 weeks of degradation in vitro.

infiltration of surrounding tissues in the PLLA nanofiber mat. Inflammatory reaction at the early stage may be due to the acidic low-molecular-weight degradation products and fragmented nanofibers.

A different situation was observed for the stereocomplexed PLA nanofibers. It is supposed that a single stereocomplexed PLA nanofiber is composed of PLLA and PDLA chains aligned

in a side-by-side manner. Accordingly, it is well-known that molecular interaction between PLLA and PDLA chains is strong, leading to higher melting temperature. Such molecular arrangement may suppress the hydrolysis of molecular chains in vivo. Thus, the stereocomplexed nanofiber morphology is retained. As a result, inflammatory reaction is limited at the vicinity of the interfacial region between nanofiber mats and the surrounding tissues.

General Discussion. Physiological response of tissues against implanted foreign materials is one of the most significant subjects to be considered in the development of medical biomaterials. In the case of polymeric biomaterials, the degree of the tissue responses, such as inflammatory reactions, partly depends on the chemical structure and, as a consequence, surface hydrophilic nature of the polymers.[23] Additionally, for biodegradable polymers, the degree of tissue responses is affected by the degradability in vivo.[24] For example, poly(glycolic acid) that undergoes degradation in vivo generally in 2−4 weeks is known to cause acute inflammatory reaction as the degradation proceeds.[25] It is known that the hydrolysis by body fluids is the major mechanism contributing in vivo degradation of polymeric biomaterials. We have already shown that the degradation behavior of poly(hydroxyalkanoate)s (PHAs) in vivo are largely affected by the monomer composition.[26] Nanofiber scaffolds made from these PHAs, ranging from poly[(*R*)-3-hydroxybutyrate] to poly[(*R*)-3-hydroxybutyrate-*co*-97 mol %-4-hydroxybutyrate] lead to contrasted tissue responses. The tissue responses were well correlated with the degradability of each polymer scaffolds. The present study using nanofibers of PLLA and stereocomplexed PLA suggested the correlation between the degree of inflammatory reaction in vivo and the change in the bulk size of each nanofiber mats. The changes in bulk size of the nanofibers were correlated to the changes in the microscopic morphology, crystallinity, and molecular weight. All these factors give evidence that the stereocomplexed PLA nanofibers are more stable and thus provoke lower degree of inflammation in vivo than the PLLA nanofibers.

In general, inflammatory reaction is favored in the case where healing occurs in a short period of time. For example, inflammatory reaction stimulates and accelerates the regeneration of some kinds of epithelial tissues. On the other hand, in the case where healing requires a longer time, chronic inflammatory response is not favored. For example, suppression of the inflammatory responses against artificial vessel has significance for treatment of the circulatory organs that requires a period of more than half a year. From this viewpoint, our results show that the stereocomplexed PLA nanofibers are suitable for the purposes where the chronic inflammatory reaction should be avoided, for example, guided nerve regeneration or blood vessel augmentation. On the other hand, conventional PLLA nanofibers may be suitable for the rapidly bioresorbable materials, for example, wound healing patches. Such versatility of the biodegradability would expand the potential of PLAs as biomaterials.

Conclusion

Fiber morphology, crystallinity, and molecular weight of PLLA and stereocomplexed PLA nanofibers before and after implantation in vivo were investigated using SEM, WAXD, and GPC. The stereocomplexed PLA nanofiber retained its fiber morphology, crystallinity, and molecular weight after a 12 week implantation. On the other hand, the PLLA nanofiber showed breakdown of the fiber morphology and significant decrease in crystallinity and molecular weight. The degree of inflammatory reaction against the nanofibers in vivo was correlated to the degradation behavior. The larger stability against hydrolysis of stereocomplexed PLA nanofiber, attributed to the strong interaction between PLLA and PDLA chains in the nanofiber, was confirmed by in vitro degradation.

Acknowledgment. This work has been supported by a grant provided for Ecomolecular Research II in RIKEN Institute (The Institute of Physical and Chemical Research), Japan, and by a Grant-in-Aid from the Ministry of Education, Culture, Sports, Science and Technology, Japan (No. 19350075, to T.I.). We thank Ms. Noreen Fundador for the English correction of our manuscript.

References and Notes

(1) Langer, R.; Vacanti, J. P. *Science* **1993**, *260*, 920–926.
(2) Reneker, D. H.; Chun, I. *Nanotechnology* **1996**, *7*, 216–223.
(3) Morota, K.; Matsumoto, K.; Mizukoshi, T.; Konosu, Y.; Minagawa, M.; Tanioka, A.; Yamagata, Y.; Inoue, K. *J. Colloid Interface Sci.* **2004**, *279*, 484–492.
(4) Murugan, R.; Ramakrishna, S. *Tissue Eng.* **2006**, *12*, 435–447.
(5) Buchko, C. J.; Chen, L. C.; Shen, Y.; Martin, D. C. *Polymer* **1999**, *40*, 7397–7407.
(6) Zong, X.; Kim, K.; Fang, D.; Ran, S.; Hsiao, B. S.; Chu, B. *Polymer* **2002**, *43*, 4403–4412.
(7) Zong, X.; Ran, S.; Kim, K.-S.; Fang, D.; Hsiao, B.; Chu, B. *Biomacromolecules* **2003**, *4*, 416–423.
(8) Ikada, Y.; Tsuji, H. *Macromol. Rapid Commun.* **2000**, *21*, 117–132.
(9) Iwata, T.; Doi, Y. *Sen'i Gakkaishi* **2001**, *57*, 172–177.
(10) Ikada, Y.; Jamshidi, K.; Tsuji, H.; Hyon, S. H. *Macromolecules* **1987**, *20*, 904–906.
(11) Tsuji, H. *Macromol. Biosci.* **2005**, *5*, 569–597.
(12) Okihara, T.; Tsuji, M.; Kawaguchi, A.; Katayama, K.; Tsuji, H.; Hyon, S. H.; Ikada, Y. *J. Macromol. Sci., Part B: Phys.* **1991**, *30*, 119–140.
(13) Tsuji, H. *Polymer* **2000**, *41*, 3621–3630.
(14) Tsuji, H.; Suzuki, M. *Sen'I Gakkaishi* **2001**, *57*, 198–202.
(15) Tsuji, H.; Miyaushi, S. *Biomacromolecules* **2001**, *2*, 597–604.
(16) Takasaki, M.; Ito, H.; Kikutani, T. *J. Macromol. Sci., Part B: Phys.* **2003**, *42*, 57–73.
(17) Furuhashi, Y.; Kimura, Y.; Yamane, H. *J. Polym. Sci., Part B: Polym. Phys.* **2007**, *45*, 218–228.
(18) Tsuji, H.; Nakano, M.; Hashimoto, M.; Takashima, K.; Katsura, S.; Mizuno, A. *Biomacromolecules* **2006**, *7*, 3316–3320.
(19) Ishii, D.; Lee, W.-K.; Kasuya, K.-I.; Iwata, T. *J. Biotechnol.* **2007**, *132*, 318–324.
(20) Kim, K.; Yu, M.; Zong, X.; Chiu, J.; Fang, D.; Seo, Y.-S.; Hsiao, B. S.; Chu, B.; Hadjiargyrou, M. *Biomaterials* **2003**, *24*, 4977–4985.
(21) Zeng, J.; Chen, X.; Liang, Q.; Xu, X.; Jing, X. *Macromol. Biosci.* **2004**, *4*, 1118–1125.
(22) You, Y.; Min, B.-M.; Lee, S. J.; Lee, T. S.; Park, W. H. *J. Appl. Polym. Sci.* **2005**, *95*, 193–200.
(23) Wang, Y.-X.; Robertson, J. L.; Spillman, W. B.; Claus, R. O. *Pharm. Res.* **2004**, *21*, 1362–1373.
(24) Hasirci, V.; Lewandrowski, K.; Gresser, J. D.; Wise, D. L.; Trantolo, D. J. *J. Biotechnol.* **2001**, *86*, 135–150.
(25) Ceonzo, K.; Gaynor, A.; Shaffer, L.; Kojima, K.; Vacanti, C. A.; Stahl, G. A. *Tissue Eng.* **2006**, *12*, 301–308.
(26) Tan, H. Y.; Ishii, D.; Mahara, A.; Murakami, S.; Yamaoka, T.; Sudesh, K.; Samian, R.; Fujita, M.; Maeda, M.; Iwata, T. *Biomaterials* **2008**, *29*, 1307–1317.

BM8009363

Intracellular Enzyme-responsive Fragmentation of Nonviral Gene Carriers Leads to Polyplex Destabilization and Enhanced Transgene Expression

Tomoko Hashimoto,[1,2] Yoichi Tachibana,[1] Hisae Nozaki,[1] Osam Mazda,[3]
Takuro Niidome,[4] Akira Murakami,[2] and Tetsuji Yamaoka*[1]
[1]*Department of Biomedical Engineering, National Cardiovascular Center Research Institute, 5-7-1 Fujishirodai, Suita, Osaka 565-8565*
[2]*Department of Biomolecular Engineering, Kyoto Institute of Technology, Matsugasaki, Sakyo-ku, Kyoto 606-8585*
[3]*Department of Microbiology, Kyoto Prefectural University of Medicine, Kawaramachi-Hirokoji, Kamikyo-ku, Kyoto 602-8566*
[4]*Department of Applied Chemistry, Faculty of Engineering, and Center for Future Chemistry, Kyushu University, 744 Moto-oka, Nishi-ku, Fukuoka 819-0395*

(Received May 8, 2009; CL-090444; E-mail: yamtet@ri.ncvc.go.jp)

A novel cationic oligopeptide has been developed for bioprocessing-triggered nonviral gene delivery systems. Intracellular fragmentation of the carrier in response to endogenous enzyme, furin, led to destabilized polyplexes and enhanced transgene expression.

Various nonviral polymeric gene carriers have been recently proposed for effective gene transfer but are also known to inhibit the transcription efficiency in nuclei due to the strong polyplex compaction. The polyplex compaction is affected by various physical properties of carriers, such as hydrophobicity, hydrophilicity, and molecular weight (MW). Many researchers have been investigating the effect of carrier MW on transfection efficiency.[1–4] Godbey et al. reported that MW 70000 poly(ethyleneimine) (PEI) produced much higher expression levels than low MW PEI in cell culture because of better entry of polyplexes into the cells or stronger protection of pDNA.[1] On the other hand, Schaffer et al. reported that pDNA is dissociated from lower MW poly(L-lysine) more rapidly and that the weak interaction permits larger transcription rate in a cell-free system.[3] According to these findings, intracellular fragmentation of carriers is suspected to result in effective transfection because of the better entry of transgene and the higher transcription rate.

In this work, we designed oligopeptide-type nonviral carriers (Fur-oligopeptides) containing a cleavable sequence for intracellular proprotein convertase, furin. Furin is related to the processing of a wide variety of protein precursors within the secretory pathway and localized at trans-Golgi network, lysosome, and endosome of a broad range of mammalian cells.[5,6] It has been reported that furin recognizes the cleavage-site sequence Arg–X–X–Arg (R–X–X–R).[7] Especially, highly cationic Arg–X–(Lys/Arg)–Arg (R–X–(K/R)–R) is cleaved with 10-fold higher efficiency than R–X–X–R. Fur-oligopeptide, which has a repeating R–X–(K/R)–R sequence, is cationic enough to form polyplexes with nucleic acids electrostatically and to deliver nucleic acids into cells. Fur-oligopeptide is expected to be fragmented in an intracellular environment and lead to high transgene expression by releasing pDNA.

Fur-oligopeptides were synthesized by stepwise elongation of Fmoc amino acids on solid-phase resins. $(RKRKKR)_4C$ has seven cleavage sites.[8] $(RKRKRK)_4C$ is a control sequences without cleavage site. RKKR is a model peptide for the digested fragment.

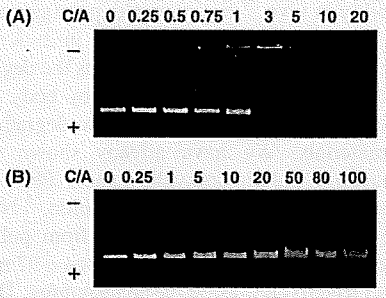

Figure 1. EtBr stained agarose gel (0.8%) electrophoresis of $(RKRKKR)_4C$/pT7-Luc (A) and RKKR/pT7-Luc (B) polyplexes at various C/A ratios.

$(RKRKKR)_4C$ formed polyplexes with pDNA completely at C/A ratio of 3 and above (Figure 1A). $(RKRKRK)_4C$ showed the same result (data not shown). On the other hand, RKKR formed polyplex at C/A ratio of higher than 100 (Figure 1B). Mascotti et al. calculated the equilibrium binding constant between oligolysine with various lengths and pDNA by measuring the thermodynamic extent of counter ion release resulted from the polyplex formation.[9] The equilibrium binding constant rapidly increased with increasing oligolysine length. The thermodynamic results support the large difference in polyplex-forming ability of $(RKRKKR)_4C$ (25mer) and RKKR (4mer). These results indicated that Fur-oligopeptide would lose the polyplex-forming ability and release the pDNA when fragmented in cells, which is expected to lead to high gene expression.

Polyplexes must be positively charged for better entry into cells. We measured ζ potential of $(RKRKKR)_4C$ or RKKR polyplexes. ζ Potentials of $(RKRKKR)_4C$ polyplexes were around +20 mV at a C/A ratio of 3, while RKKR polyplexes showed negative ζ potential up to a C/A ratio of 100 (data not shown). The ζ potential of $(RKRKKR)_4C$ polyplexes is similar to that of PEI/pDNA polyplexes and seems to be enough for gene delivery.[4]

Transient expressions of luciferase gene transfected with Fur-oligopeptides were evaluated. Polyplex solutions were incubated with COS-1 cells for 5 h in the presence of 200 μM chloroquine. Supernatants were removed and replaced with DMEM containing 10% FBS and then cells were cultured for 43 h. Luciferase count per second (CPS) of cells were measured using a luminometer. Obtained luciferase activities were divided by total

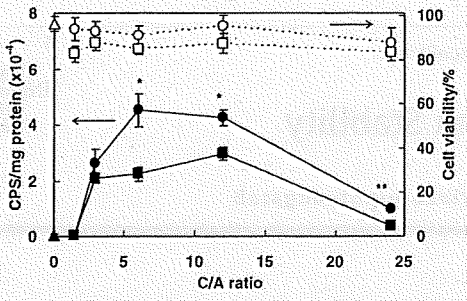

Figure 2. Transient luciferase expression (closed symbols) and cell viability (open symbols) in COS-1 cells transfected using $(RKRKKR)_4C$ (circles) and $(RKRKRK)_4C$ (squares) for 5 h in the presence of 200 μM chloroquine. (Triangles) represents the results for naked pCMV-Luc ($^*P < 0.01$, $^{**}P < 0.001$).

protein content of the cell lysates and expressed as CPS/mg protein (Figure 2). Cell viability was also assessed by the total protein in each cells. As is clearly shown, $(RKRKKR)_4C$ showed improved luciferase expression compared with a control $(RKRKRK)_4C$ with the same MW and amino acid composition. No cytotoxicity was observed in both cases. $(RKRKKR)_4C$ sequences in polyplexes is believed to be digested by intracellular furin, and this sequence-specific digestion brought about the polyplex destabilization.

We investigated the destabilization of Fur-oligopeptides/pDNA polyplexes in response to the digestion by furin in a cell-free system. Fur-oligopeptides were mixed with 200 ng pDNA in furin digestion buffer at C/A = 5 and incubated for 30 min. Five units of furin were added to 8 μL polyplex solutions and incubated for 1, 6, 12, and 24 h at 37 °C. Destabilization of polyplexes was evaluated by two experiments shown below. First, we perfomed anion-exchange assay with 0.5 equiv of potassium poly(vinyl sulfate) (PVS-K). When PVS-K was added to polyplex solutions, pDNA is replaced with PVS-K, and free pDNA is released. Reaction mixtures containing the free DNA were analyzed on EtBr-stained agarose gel (0.8%) electrophoresis. EtBr showed high fluorescence intensity by intercalating in free pDNA (Figure 3, Lane 1) but the intensity is completely suppressed when mixed with $(RKRKKR)_4C$/pDNA polyplexes because of their strong compaction (Figure 3, Lane 2). The fluorescence intensity was recovered by treating polyplexes with furin, and the intensity increased with the incubation time due to loosed compaction (Figure 3, Lane 3–6). Furthermore, release of free pDNA from digested polyplexes was observed, when the furin reaction time was longer than 12 h. Second, we evaluated the transription efficiency of the furin-treated polyplexes using an in vitro transcription/translation assay. Luciferase activity for $(RKRKKR)_4$/pT7-Luc polyplexes were increased to 30- and 100-fold after furin treatment for 1 and 6 h, respectively.[10] These results suggested that the enhanced gene expression shown in Figure 2 was resulted from the destabilization of highly compacted polyplex by intracellular furin digestion.

Katayama et al. reported polymeric carriers including substrates for protein kinase.[11] The substrate was phosphorylated by kinase, and then the charge of carriers decreased. As a result, the carriers lose polyplex-forming ability with pDNA, and GFP expression in NIH-3T3 cells was enhanced in response to the forskolin stimulation. However, since the positive charge density

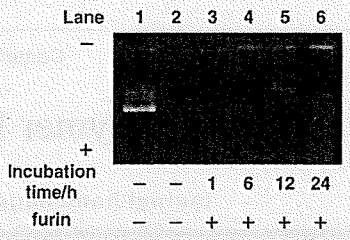

Figure 3. PVSK-induced disassembly of polyplexes treated with furin for 0, 1, 6, 12, and 24 h. Lane 1: free pCMV-Luc; lanes 2–6: $(RKRKKR)_4C$/pCMV-Luc polyplexes.

of this carrier is very low, the carrier cannot deliver pDNA into cells by itself and needs HVJ-E envelope. In contrast, $(RKRKKR)_4C$ can deliver pDNA into cells by itself and is fragmented to short peptides in response to intracellular furin. Other groups have reported biodegradable PEI derivatives.[12,13] These carriers might also facilitate intracellular release of pDNA from polyplexes, but remaining low MW PEI fragments are still non-biodegradable as is different from our Fur-oligopeptides.

In general, oligopeptide-type carriers have a high potential for useful gene carriers because various types of functional sequences such as receptor-binding sequences, NLS sequences, and digestive sequences can be combined. Increasing the MW of the carrier might be effective for pDNA delivery to cells[5] but higher MW carriers are reported to be more cytotoxic than the lower MW ones.[4] The optimum MW of Fur-oligopeptides are now studying.

In conclusion, Fur-oligopeptide has been newly developed as a gene carrier which is fragmented by intracellular furin, and the destabilized polyplexes are effectively transcibed in cells. This intracellular fragmentation of cationic carriers is a novel strategy for non-viral gene delivery.

This work was supported by Grants for Regional Science and Technology Promotion from the Ministry of Education, Culture, Sports, Science and Technology.

References and Notes

1 W. T. Godbey, K. K. Wu, A. G. Mikos, *J. Biomed. Mater. Res.* **1999**, *45*, 268.
2 P. Symonds, J. C. Murray, A. C. Hunter, G. Debska, A. Szewczyk, S. M. Moghimi, *FEBS Lett.* **2005**, *579*, 6191.
3 D. V. Schaffer, N. A. Fidelman, N. Dan, D. A. Lauffenburger, *Biotechnol. Bioeng.* **2000**, *67*, 598.
4 K. Kunath, A. V. Harpe, D. Fischer, H. Petersen, U. Bickel, K. Voigt, T. Kissel, *J. Controlled Release* **2003**, *89*, 113.
5 K. Hatsuzawa, M. Hosaka, T. Nakagawa, M. Nagase, A. Shoda, K. Murakami, K. Nakayama, *J. Biol. Chem.* **1990**, *265*, 22075.
6 S. S. Molloy, L. Thomas, J. K. VanSlyke, P. E. Stenberg, G. Thomas, *EMBO J.* **1994**, *13*, 18.
7 M. Hosaka, M. Nagahama, W. S. Kim, T. Watanabe, K. Hatsuzawa, J. Ikemizu, K. Murakami, K. Nakayama, *J. Biol. Chem.* **1991**, *266*, 12127.
8 T. Hashimoto, A. Murakami, T. Yamaoka, *Nucleic Acids Symp. Ser.* **2004**, *48*, 235.
9 D. P. Mascotti, T. M. Lohman, *Proc. Natl. Acad. Sci. U.S.A.* **1990**, *87*, 3142.
10 Supporting Information is available electronically on the CSJ-Journal Web site, http://www.csj.jp/journals/chem-lett/index.html.
11 Y. Katayama, K. Fujii, E. Ito, S. Sakakihara, T. Sonoda, M. Murata, M. Maeda, *Biomacromolcules* **2002**, *3*, 905.
12 C.-H. Ahn, S. Y. Chae, Y. H. Bae, S. W. Kim, *J. Control. Release* **2002**, *80*, 273.
13 G. P. Tang, H. Y. Guo, F. Alexis, X. Wang, S. Zeng, T. M. Lim, J. Ding, Y. Y. Yang, S. Wang, *J. Gene Med.* **2006**, *8*, 736.

Published on the web (Advance View) June 13, 2009; doi:10.1246/cl.2009.718